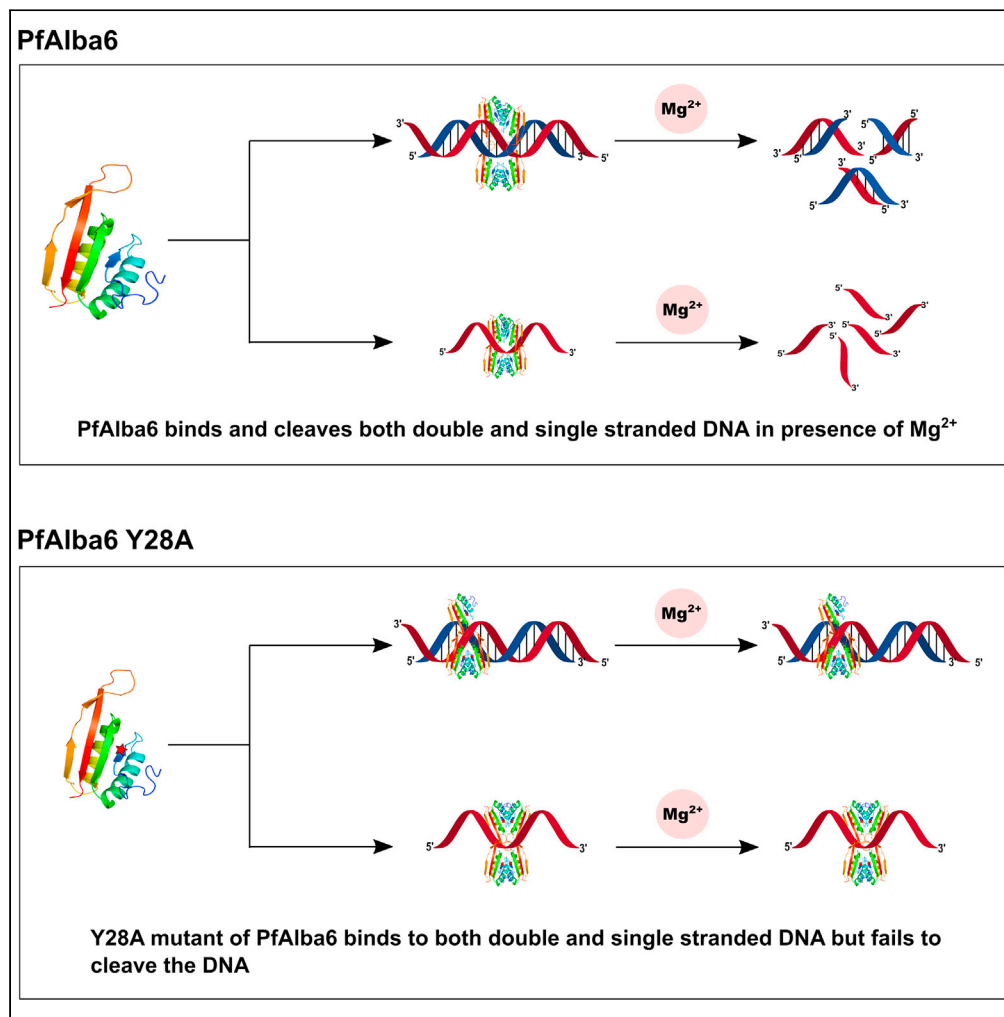


Article

Plasmodium falciparum Alba6 exhibits DNase activity and participates in stress response

Shiladitya Nag,
Chinmoy Banerjee,
Manish Goyal, ...,
Shubhra Jyoti
Saha, Rudranil De,
Uday
Bandyopadhyay

ubandyo_1964@yahoo.com

Highlights

PfAlba6 exhibits Mg^{2+} -dependent DNase activity in 5'-to-3' polarity

Tyrosine28 plays a pivotal role in PfAlba6 DNase activity

PfAlba6 oligomerizes while binding DNA at high concentration

Artemisinin and heat-induced stress upregulate PfAlba6 mRNA expression

Nag et al., iScience 27, 109467
April 19, 2024 © 2024 The
Author(s).
[https://doi.org/10.1016/
j.isci.2024.109467](https://doi.org/10.1016/j.isci.2024.109467)

Article

Plasmodium falciparum Alba6 exhibits DNase activity and participates in stress response

Shiladitya Nag,¹ Chinmoy Banerjee,¹ Manish Goyal,² Asim Azhar Siddiqui,¹ Debanjan Saha,¹ Somnath Mazumder,^{1,3} Subhashis Debsharma,¹ Saikat Pramanik,¹ Shubhra Jyoti Saha,¹ Rudranil De,⁴ and Uday Bandyopadhyay^{1,5,6,*}

SUMMARY

Alba domain proteins, owing to their functional plasticity, play a significant role in organisms. Here, we report an intrinsic DNase activity of PfAlba6 from *Plasmodium falciparum*, an etiological agent responsible for human malignant malaria. We identified that tyrosine28 plays a critical role in the Mg²⁺ driven 5'-3' DNase activity of PfAlba6. PfAlba6 cleaves both dsDNA as well as ssDNA. We also characterized PfAlba6-DNA interaction and observed concentration-dependent oligomerization in the presence of DNA, which is evident from size exclusion chromatography and single molecule AFM-imaging. PfAlba6 mRNA expression level is up-regulated several folds following heat stress and treatment with artemisinin, indicating a possible role in stress response. PfAlba6 has no human orthologs and is expressed in all intra-erythrocytic stages; thus, this protein can potentially be a new anti-malarial drug target.

INTRODUCTION

Malaria is one of the deadliest tropical diseases and claims millions of lives all over the world.¹ Advancement of genomic research and combinatorial therapeutics initially curbed the deadliness of the disease.² Still, the rapid emergence of drug-resistant *Plasmodium* sp. urgently needs more effective and advanced anti-malarial pharmacotherapeutics.³⁻⁷ The emergence of resistant *Plasmodium* sp. is much faster than the invention of new therapeutics; therefore, improved strategies for identifying new drug targets require urgent attention.⁸ First-line anti-malarial drugs like chloroquine, mefloquine, Malarone, and artemisinin instigate parasite genome instability and culminate in apoptosis-like death.⁹⁻¹¹ Various studies have proposed that artemisinin has multiple cellular targets involving reactive oxygen species (ROS), which leads to oxidative stress in the parasites.¹² *Plasmodium falciparum* has a plethora of DNA damage repair proteins to protect its unique structural organization.¹³⁻¹⁵ Available genome information of *P. falciparum* facilitated us uncovering those putative parasite proteins, which are highly conserved in parasites with no human orthologs and are essential for drug-induced DNA stress response. Thus, they may serve as promising drug targets. Interestingly, the *Plasmodium* genome is 82% A + T rich, higher than any other organism.¹⁶ We investigated the DNA-interacting protein families of *P. falciparum* to understand how the parasite nucleic acid functions with such a unique genomic makeup.¹⁶⁻²⁰

Apart from histones, the *Plasmodium* genome encodes a unique DNA-RNA binding protein family, crucial for maintaining genetic and epigenetic functions under such unique genome organization.²¹⁻²⁷ Previously, genomic and transcriptomics data identified nuclear proteins from the *P. falciparum* genome that are small, basic and dimeric, belonging to the Alba (Acetylation Lowers Binding Affinity) superfamily. The Alba proteins came into the limelight after their identification as sequence-independent DNA binding proteins from archaeal hyper-thermophiles.²⁸⁻³⁰ It has been proposed that Alba's acetylation occurs reversibly, with the non-acetyl form having greater affinity toward the DNA.²⁸⁻³¹ In *Sulfolobus solfataricus*, the acetylation and deacetylation are catalyzed by a homolog of Pat (protein acetyltransferase) and Sir2 protein (a sirtuin family NAD-dependent deacetylase), respectively.^{28,32,33} Both in Euryarchaea (histone present) and Crenarchaea (histone absent), Alba proteins are a significant architectural DNA binding protein, playing an essential role in the organization and regulation of the genome.^{29,34-36} However, studies have revealed that these Alba proteins are also associated with the RNA through the arginine-glycine-glycine repeat (RGG) present at the C terminal region where binding is modulated by methylation at the arginine in the RGG box.^{34,37-44} Alba protein is not restricted to the Archaeal family and plants possess this protein where it plays important roles in oxidative stress tolerance.^{45,46}

¹Division of Infectious Diseases and Immunology, CSIR-Indian Institute of Chemical Biology, 4, Raja S. C. Mullick Road, Jadavpur, Kolkata 700032, West Bengal, India

²Department of Molecular & Cell Biology, School of Dental Medicine, Boston University Medical Campus, Boston, MA, USA

³Department of Zoology, Raja Peary Mohan College, 1 Acharya Dhruva Pal Road, Uttarpara, West Bengal 712258, India

⁴Amity Institute of Biotechnology, Amity University, Kolkata, Plot No: 36, 37 & 38, Major Arterial Road, Action Area II, Kadampukur Village, Newtown, Kolkata, West Bengal 700135, India

⁵Division of Molecular Medicine, Bose Institute, Unified Academic Campus, EN 80, Sector V, Bidhan Nagar, Kolkata, West Bengal 700091, India

⁶Lead contact

*Correspondence: ubandyo_1964@yahoo.com

<https://doi.org/10.1016/j.isci.2024.109467>



Alba proteins bind cooperatively to dsDNA, ssDNA and DNA-RNA hybrid⁴⁶ in a sequence-independent manner without significant compaction⁴⁷ and are distributed uniformly in chromosomes.²⁸ Recent studies have revealed that this protein family exhibited nuclease activity with different propensities.⁴⁸ A genome-wide search has identified six paralogs of DNA-RNA binding protein belonging to the Alba superfamily in *P. falciparum* that might play an essential role in parasite stress regulation. Among these, four have already been characterized. They bind to the hyper-repetitive telomere-associated repeat element 6 (TARE 6) region of the subtelomeric region (at the minor groove of the DNA). They are distributed in the nuclear periphery in the nucleus and the cytoplasm.^{39,49} PfAlba3 has been shown to possess an apurinic/aprimidinic site-driven intrinsic nuclease activity to dsDNA.⁴⁸ Here, we describe PfAlba6 (Gene ID: Pf3D7_1202800), which has no human orthologs and shows Mg²⁺ dependent DNase activity at a wide range of temperature and pH. PfAlba6 can target dsDNA and ssDNA independent of the presence of any abasic site. An abasic site, also known as an AP site (apurinic/aprimidinic site), is a location in DNA that lacks a purine or pyrimidine base, generated spontaneously or due to DNA damage. Furthermore, we have identified the essential role of tyrosine28 in exhibiting the DNase activity. Subsequent investigations revealed that subjecting the parasites to stress by artemisinin and elevated temperatures significantly upregulated the expression of PfAlba6 mRNA, indicating the role of this protein in *P. falciparum* stress management like other Alba superfamily proteins.

RESULTS

Molecular modeling of PfAlba6

Plasmodium falciparum PfAlba6 is a putative 96 amino acid DNA-RNA binding protein of molecular mass 11.4 kDa. Sequence alignment study reveals that PfAlba6 has no homology with human proteins. This protein has no similarity with other species of other genus except *Plasmodium* (Figure 1A). *In-silico* studies from Plasmodb.org further revealed that this protein has an Alba domain spanning 17–80 amino acid residues of the protein. PredictProtein.org predicted that it has an “alpha-beta” secondary structure with around 28% Helix, 23% strand, and 49% Loop (Table S1). About 76% of residues are exposed, with 23% buried^{50,51,52,53} (Table S1). The protein structure was predicted by I-TASSER (Figure 1B), which uses 10 templates to indicate the model (Table S2). The DNA binding site was also predicted by I-TASSER using COFACTOR and COACH predictions (Figure 1C). According to this model, the binding of PfAlba6 to the dsDNA is similar to that of Ssh10b (a member of the Sac10b family from *Sulfolobus shibatae*) to the dsRNA, with S¹⁸, I¹⁹, K²⁰, Y²⁸, R⁴⁶, Q⁴⁷, Y⁴⁸, A⁴⁹ and I⁸⁶ being the predicted nucleic acid binding sites. The stereochemical validation of the final model indicated by I-TASSER was performed at various web servers (Table S3) which agree with the accurate prediction of the PfAlba6 model as proposed by I-TASSER.

Purification and characterization of PfAlba6

PfAlba6 in pET-28 a (+) vector was overexpressed in Rosetta (DE3) pLysS *E. coli* cells. To obtain a highly purified protein, the supernatant obtained after the ultracentrifugation of the sonicated induced lysate was initially subjected to cation exchange chromatography followed by Ni-NTA column chromatography and size exclusion chromatography (HiLoad Superdex 16/600 75 pg preparative size exclusion chromatography column) in FPLC.

The purity of the protein was determined by running the concentrated protein in 15% SDS-PAGE, where a single band was obtained (Figure S1A (inset)). The protein was then subjected to MALDI-TOF MS, and a peak at ~14.9 kDa complying with the theoretical mass of the protein with the tag (Figure S1A) was obtained. Again, to identify and characterize the protein and to rule out the presence of any non-specific over-expression of protein of similar molecular mass or the presence of any contaminant protein of the same molecular mass, MALDI-TOF/TOF MSMS of in-gel tryptic digested protein was done and matched with NCBI database to obtain 100% correlation indent score.

The helicity of PfAlba6 was determined using circular dichroism (CD) to determine its secondary structure. Helical structure plays a vital role in the execution of the function of the protein. The CD spectrum shows a predominantly alpha-helical structure (Figure S1B) that corroborates well with the predicted data.^{54–57} The purified protein was then used to generate antibodies in rabbits using Freund’s adjuvants. The polyclonal antibody generated in rabbit was tested for efficacy by immunoblotting with overexpressed *E. coli* lysate and a single band was obtained at the expected position.

Stage-specific expression and localization of PfAlba6

The stage-specific expression of PfAlba6 was assessed by real-time quantitative PCR and confocal microscopy. Amplification of a 200 bp fragment of PfAlba6 was found in Real-Time quantitative PCR using cDNA from ring, trophozoite and schizont stages (Figure 2A). PfActinII (Pf3D7_1412500) was used as a reference control, expressed uniformly in all the stages. As determined through the real-time quantitative PCR, the mRNA level indicated almost an equal level of expression of PfAlba6 throughout all the asexual stages (Figure 2A). An immunofluorescence assay supported the finding, which showed that this protein is expressed in all the erythrocytic life stages. Immunofluorescence data of PfAlba6 also showed the subcellular localization of the protein during the asexual developmental cycle (Figure 2B). Confocal data indicated that PfAlba6 (Alexa Fluor 647, red) is expressed in all the intra-erythrocytic stages of the parasite and appears predominantly in cytoplasm with a small population in the nucleus (DAPI, blue).

PfAlba6 forms oligomer in the presence of DNA

The DNA binding property of the protein was evaluated by agarose gel retardation assay. The mobility of supercoiled DNA (pBR322) incubated with the protein was retarded with an increase in PfAlba6: DNA ratio (w/w); more the ratio, the more the shift (Figure 3A) clearly stating

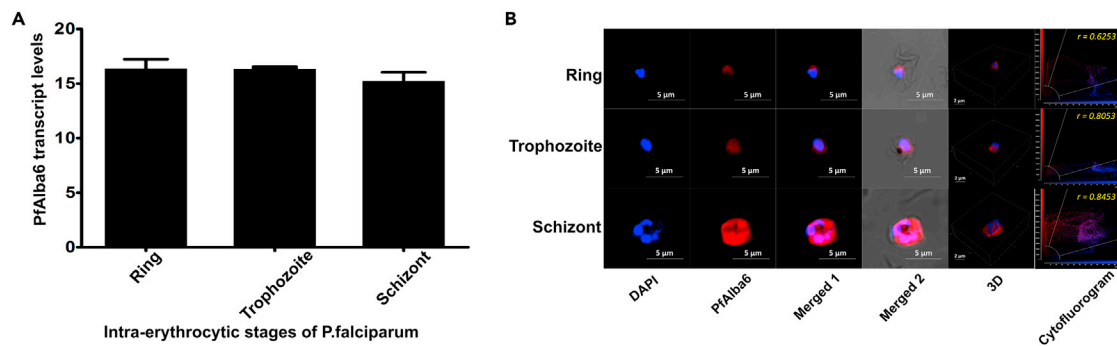


Figure 2. Stage-specific expression and localization of PfAlba6

(A) Differential expression profile of the *PfAlba6* gene in the different intra-erythrocytic stages (ring, trophozoite and schizont stages) has been performed using Real-time PCR. *PfActin11* (Pf3D7_1412500) was used as a reference control. Data are represented as mean ± SEM. n = 4 biological replicates.

(B) Stage-specific expression and subcellular localization of *PfAlba6* as observed in immunofluorescence microscopy of *PfAlba6* (Red, Alexa Fluor 647) throughout the parasite asexual blood stages (ring, trophozoite and schizont stages) with DAPI (blue) for nuclear staining. “r” indicates Pearson’s correlation coefficient between blue and red signal corresponding to *PfAlba6* and nucleus respectively. Scale bar, 5 μm and 2 μm. See also Figure S1. Representative images from three biological replicates are shown.

molecular standards (Figure 3D (inset)) clearly showed the formation of higher molecular weight oligomers. The K_d value, as determined by the BLI, is 7.9 ± 0.015 nM for the lower concentration and 10 ± 0.37 nM and 2.52 ± 0.19 μM as K_{d1} and K_{d2} , respectively, for the higher concentrations. The high value of K_{d2} denotes two types of interaction at the higher protein concentrations: protein-protein and protein-DNA. K_d value at the low concentration, which signifies protein: DNA interaction, shows that *PfAlba6* has a robust affinity for DNA.

Next molecular imaging of DNA-*PfAlba6* interaction was followed by atomic force microscopy (AFM) (Figures 4A–4C). As can be seen in the topological graph, DNA alone has a maximum height of 1.10 nm (Figure 4A). *PfAlba6* alone shows that most of the proteins have an average height of 0.5 nm, with a few oligomers having a maximum height of 0.98 nm (Figure 4B). However, upon interacting with the pBR322, it was seen that there has been a deposition of protein at certain regions where it binds to the DNA (Figure 4C). The maximum height of the protein was found to be 2.0 nm, which supports the result obtained in BLI and size-exclusion chromatography in the absence and presence of DNA that *PfAlba6* might undergo oligomerization on interacting with DNA.

PfAlba6 exhibits DNase activity

Metal ions play important roles in the interaction of the protein with the DNA. Thus, to determine the role of the divalent metal ions in the *PfAlba6*-DNA interaction, an agarose gel retardation assay was performed in the presence of an increasing concentration of different metal ions (Mg^{2+} , Ca^{2+} , Zn^{2+} , Cu^{2+} , Ni^{2+} , Mn^{2+}). Surprisingly, *PfAlba6* showed DNase activity in the presence of the divalent metal ions but with different efficacies with different metal ions. Plasmid degradation assay demonstrated a unique Mg^{2+} dependent DNase activity of *PfAlba6* compared with other divalent metal ions (Figure 5A). DNA degradation decreased with increasing concentrations of EDTA and was eventually inhibited by 20 mM EDTA (Figure 5B). However, EGTA could not block its activity even at a high concentration of 100 mM (Figure 5C), which further confirmed the Mg^{2+} dependency of the activity. *PfAlba6* showed concentration-dependent DNase activity when it could degrade supercoiled pBR322 with its increasing concentration (Figure 5D). It was found that 2.5 μg of *PfAlba6* could completely cleave 250 ng of pBR322. *PfAlba6* showed DNase activity at neutral to higher pH but not in the lower pH (Figure 6A) and at a wide temperature range (Figure 6B). The nuclease activity of *PfAlba6* was monitored using C28 DNA and staining it with Invitrogen SYBR Safe DNA Gel Stain to measure different kinetic parameters ($V_{max} = 1.3 \pm 0.07 \times 10^6$ A.U. hr^{-1} , $K_M = 93.5 \pm 13.19$ p.m. and $k_{cat} = 7.085 \pm 0.38 \times 10^{-5}$ hr^{-1}) (Figure 6C). The mechanism of this activity can be predicted only after deciphering the residues involved in the DNase activity of *PfAlba6*.

PfAlba6 cleaves DNA in 5'-3' direction

The DNase activity using pBR322 is complicated due to the different forms of DNA (closed circular, linear or nicked species). To add to this, pBR322 might also have damaged bases in it. So, to be more specific about the function of *PfAlba6*, we used a small linear of 28bp DNA to determine the exact mechanism of its activity. Autoradiography showed that endonucleases Endo III and Endo IV are unable to cleave the C28 DNA having no abasic sites, whereas *PfAlba6* and DNase I can cleave, showing that *PfAlba6* might have an activity similar to that of DNase I (Figures 7A and 7B). On comparing the DNase activity of *PfAlba6* with *PfAlba3*, another Alba family protein from *P. falciparum*, it showed that it does not possess any AP (apurinic/aprimidinic) endonuclease activity on comparing its activity with Endo III and Endo IV over THF28 unlike *PfAlba3* when a band similar to that of C28 was observed (Figure 7C). It is known that THF28 DNA mimics the abasic site, which can be cleaved by Endo IV and *PfAlba6* and follows the hydrolysis mechanism but not by Endo III, which follows the β-elimination reaction. Moreover, *PfAlba6* was even able to cleave ssDNA (Figure 7D). On further analysis, by comparing the DNase activity of *PfAlba6* with that of DNase I over 3'-C28, the mechanisms of action of the two were found to be different, as is evident from the position of the product bands. Moreover, the data

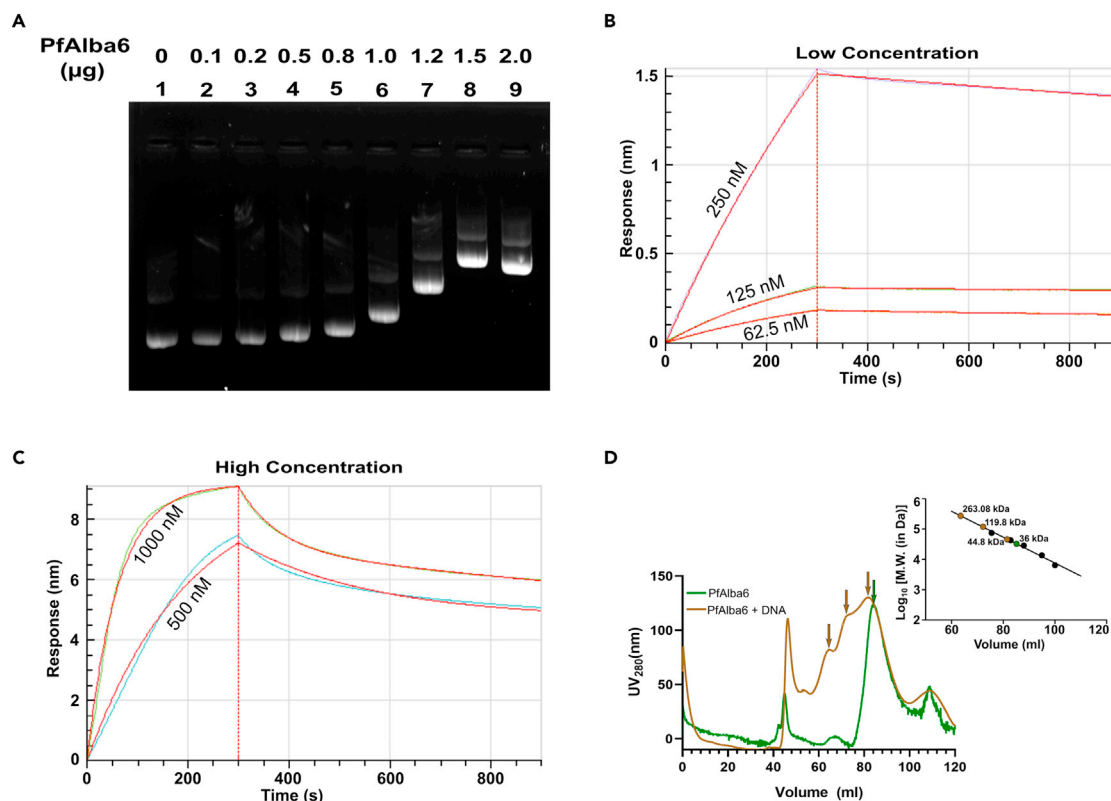


Figure 3. Assessment of the DNA binding property of PflAlba6

(A) Agarose gel shift assay. The protein interacts with DNA (pBR322) retarding the mobility of the plasmid in the 1% agarose gel. Lane 1: control plasmid (250 ng pBR322 with buffer), Lane 2–9: 250 ng of pBR322 with increasing concentrations of PflAlba6 (0.1 μ g, 0.2 μ g, 0.5 μ g, 0.8 μ g, 1 μ g, 1.2 μ g, 1.5 μ g, 2 μ g respectively). Representative images from three technical replicates are shown.

(B and C) Biolayer Interferometry (BLI) analysis of the PflAlba6–DNA interaction. 5 different concentrations of PflAlba6 (62.5 nM, 125 nM, 250 nM, 500 nM, 1000 nM) were subjected to BLI analysis. BLI was performed at 25°C in the BLI-buffer (25 mM Tris, 50 mM NaCl, pH: 7.5). A 28 bp biotinylated dsDNA (44 μ g/mL) was immobilized onto streptavidin-coated biosensor as the bait. Shown are the representative sensorgrams from three independent experiments. The graphs show the association step for the first 300 s, and then the sensors were transferred to buffer-containing wells to measure dissociation (B) for (C top) low and (C down) high PflAlba6 concentrations. The red lines (C) depict the best-fit line as predicted by the software. Individual BLI data points were taken every 0.2 s. The data were processed and analyzed with the Octet Data Analysis Software. A control without PflAlba6 was subtracted from the remainder of the data collected. Representative images from three technical replicates are shown.

(D) Chromatogram of size-exclusion chromatography of PflAlba6 in the presence (brown line) and absence (green line) of the 28 bp DNA. Size exclusion was performed in Cytiva Akta Pure system using HiLoad Superdex 16/600 75 μ g preparative size exclusion chromatography column. The arrows represent the peak volumes of elution. **Inset:** The average molecular mass of PflAlba6, both in the presence and absence of DNA, was determined by plotting the mass on the standard curve. The standard curve was obtained by plotting logarithm (base 10) of molecular mass (in Da) of the standards (Aprotinin: 6,500 Da; Ribonuclease A: 13,700 Da; Carbonic anhydrase: 29,000 Da; Ovalbumin: 43,000 Da; Conalbumin: 75,000 Da) against volume of their respective elution through the same column keeping the parameters same as that was used for PflAlba6 elution. Shown is the representative chromatogram from three replicates.

showed that the DNase activity of PflAlba6 has a 5'→3' directionality as multiple bands were obtained in the case of 3'-labelled DNA, whereas a single band was obtained in the case of 5'-labelled DNA (Figure 7E).

Tyrosine28 is essential for DNase activity

Site-directed mutagenesis of PflAlba6 was performed based on the predictions by I-TASSER. The DNase activity of PflAlba6 in comparison to its mutations was performed using FAM-C28. Though DNase I, PflAlba6 and PflAlba6 del (19–21) were able to cleave the DNA, mutation at a single position of Y (Y28A) was unable to cleave the DNA, showing that the tyrosine residue at the 28th position plays a vital role in the activity of PflAlba6 (Figure 8A). Real-time DNase activity of PflAlba6 and PflAlba6 Y28A with C28 DNA were compared using PicoGreen dye assay. The data showed that while PflAlba6 protein was able to cleave the DNA with increasing time (Figure 8B), PflAlba6 Y28A was unable to do so (Figure 8C), thus further supporting the fact that the tyrosine residue at the 28th position plays an important role in the DNase activity of PflAlba6. The CD spectrum showed a similar structure to that of the wild type (Figure S2B), indicating the structural integrity of the mutant to the wild type. Further, to explore if this loss of function is not due to any binding anomaly, we measured K_d to evaluate the DNA binding of both wild

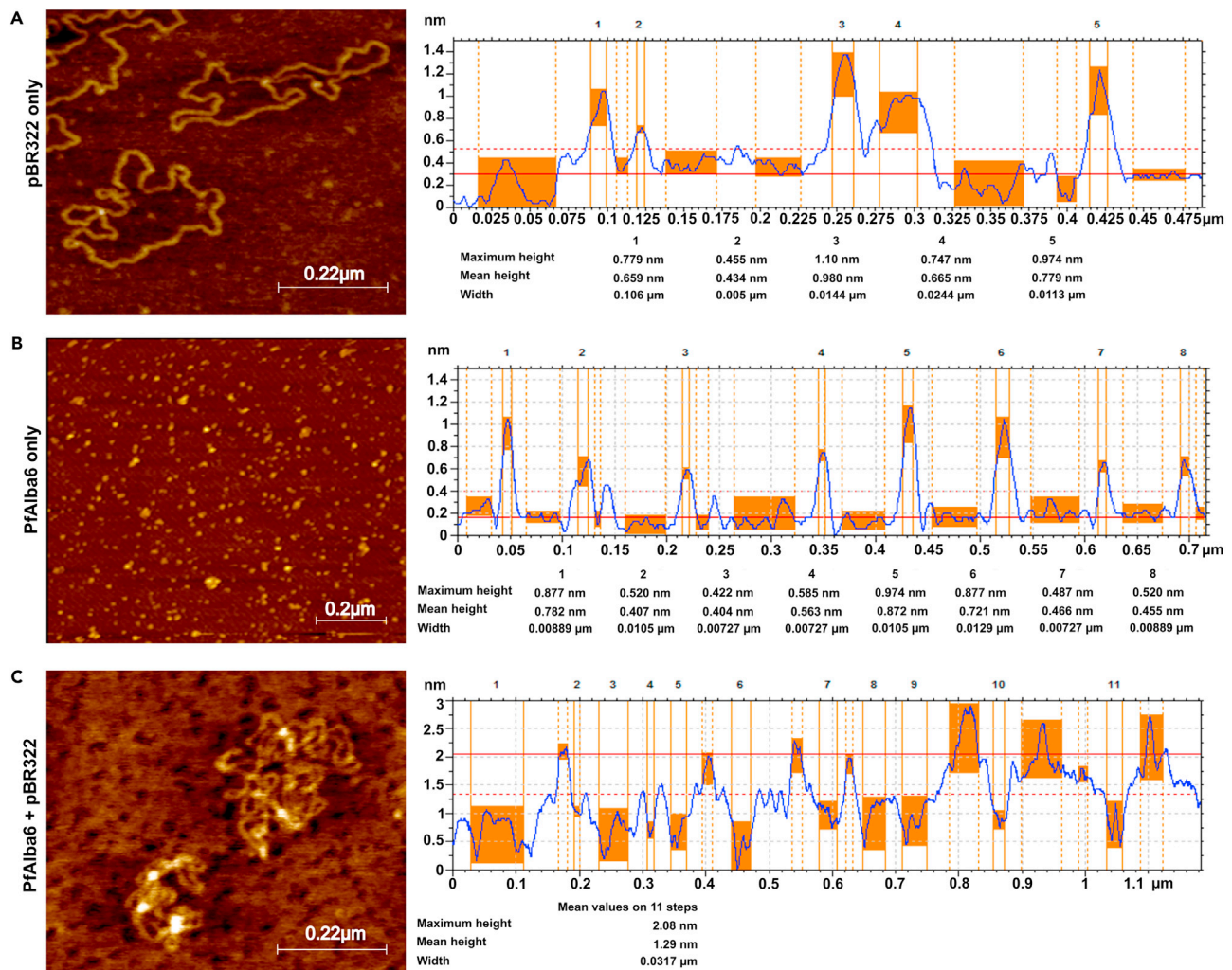


Figure 4. Atomic force microscopy (AFM) showing PfAlba6-DNA interaction

(A) Representative AFM image of 10 p.m. control pBR322 plasmid.

(B) Representative AFM image and surface profile curve of 100 nM PfAlba6.

(C) Representative AFM image and surface profile curve of PfAlba6-pBR322 complex showing aggregation of protein on interacting with DNA. The graphs represent the surface profile curve of the respective samples that shows the sample height and width obtained by arbitrarily defined extracted lines. The representative images from three technical replicates are shown.

and mutant proteins for comparison. Evaluation of DNA binding activity of PfAlba6 Y28A using BLI with 5'-Biotinylated labeled 28bp DNA indicated that the binding activity of the mutant protein (both at higher and lower concentrations) to the DNA is similar to that of the wild type (Figure 8D, inset). Just like the wild type, PfAlba6 Y28A also showed a 1:1 interaction with the DNA at lower concentration (12.14 ± 0.83 nM) (Figure S2C) and 2:1 interaction with the DNA at higher concentration ($K_{d1} = 10 \pm 0.9$ nM and $K_{d2} = 2.2 \pm 0.1$ μM) (Figure S2C). Thus indicating the loss of activity is not due to any binding anomaly. Therefore, the tyrosine residue at the 28th position plays an essential role in the DNase activity of PfAlba6. However, the detailed mechanism of this PfAlba6 activity involving the tyrosine residue is beyond the scope of the current study.

Artemisinin treatment and heat stress upregulate PfAlba6 mRNA expression

Artemisinin (ART), its derivatives (collectively referred to as ARTs), and different ART combinations are (ACTs) first-line therapies against *P. falciparum* malaria. ART treatment induces growth retardation and an accumulation of ubiquitinated proteins⁵⁸ that leads to ER stress in the parasites.⁵⁹ Artemisinin is also known to cause oxidative stress in parasites¹² by forming ROS that create genome instability in the parasite, leading to their apoptosis-like death.⁹⁻¹¹ We were interested in exploring the role and status of PfAlba6 when *P. falciparum* is under such stress. Here, we selected artemisinin as a source of stress and exposed *P. falciparum* to artemisinin to follow the status of PfAlba6. We selected

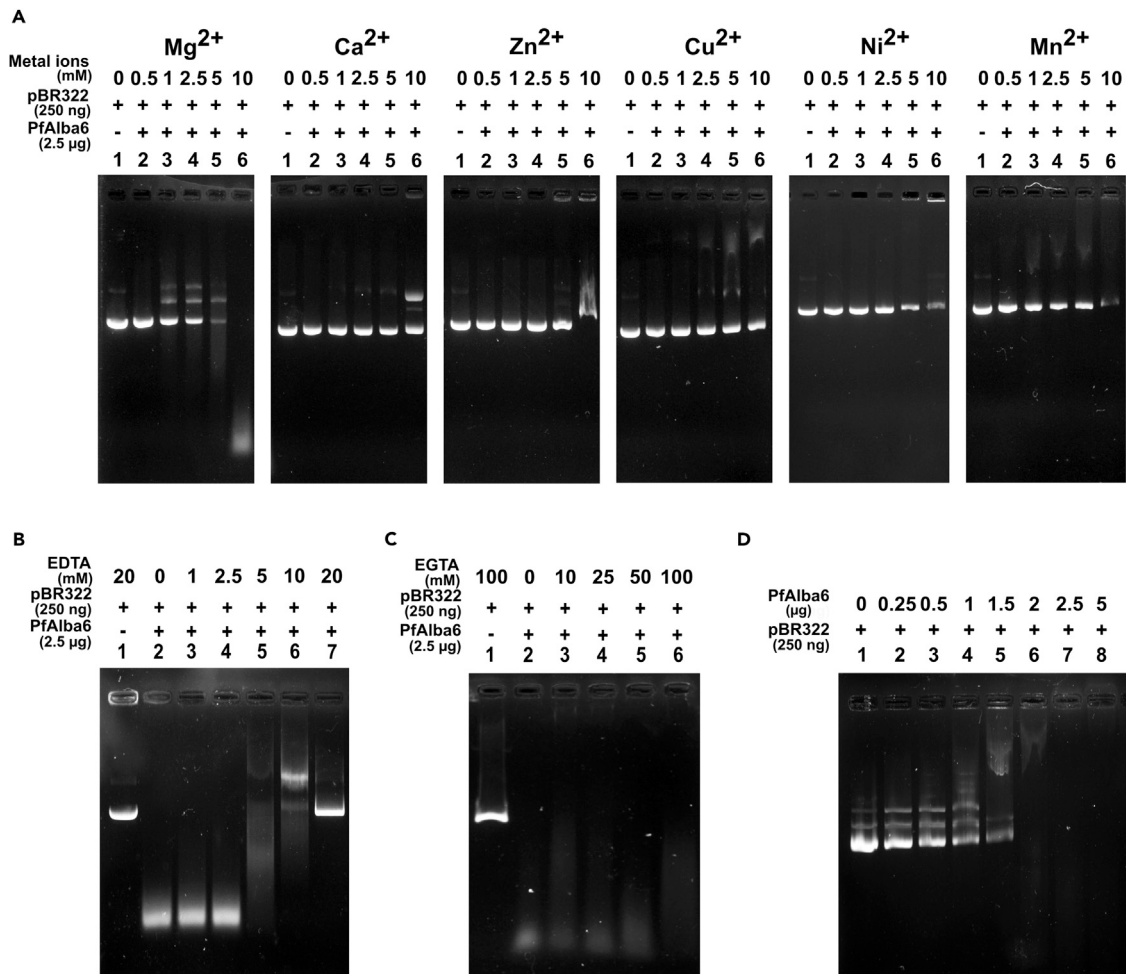


Figure 5. PflAlba6 shows nuclease activity

(A) PflAlba6 shows divalent metal ion-dependent DNase activity. Impact of different metal ions on nuclease activity of PflAlba6 was checked by DNA degradation in agarose gel in the presence of increasing concentrations of different divalent metal ions (Mg²⁺, Ca²⁺, Zn²⁺, Cu²⁺, Ni²⁺, Mn²⁺). Lane 1: Control plasmid (250 ng of pBR322 with 10 mM of the respective divalent metal ion), Lane 2–6: 250 ng of pBR322 with 2.5 μg of PflAlba6 in the presence of increasing divalent metal ions concentrations (0.5 mM, 1 mM, 2.5 mM, 5 mM, 10 mM), where PflAlba6 shows Mg²⁺ dependent DNase activity. Representative images from three technical replicates are shown.

(B and C) To confirm that the DNase activity is Mg²⁺ dependent and not Ca²⁺, DNase activity PflAlba6 was carried out in the DNase buffer containing both Mg²⁺ and Ca²⁺ with increasing concentration of (B) EDTA and (C) EGTA. Representative images from three technical replicates are shown. (B) Lane 1: control Plasmid (250 ng pBR322 in DNase buffer with 20 mM EDTA), Lane 2–7: 500 ng of pBR322 with 2.5 μg of PflAlba6 in DNase buffer with increasing concentrations of EDTA (0 mM, 1 mM, 2.5 mM, 5 mM, 10 mM, 20 mM). (C) Lane 1: control Plasmid (250 ng pBR322 in DNase buffer with 100 mM EGTA), Lane 2–7: 500 ng of pBR322 with 2.5 μg of PflAlba6 in DNase buffer with increasing concentrations of EGTA (0 mM, 10 mM, 25 mM, 50 mM, 100 mM).

(D) PflAlba6 protein shows DNase activity by cleaving pBR322 with increasing protein concentration, as depicted in 1% agarose gel. Lane 1: Control plasmid (250 ng pBR322 with DNase buffer), Lane 2–8: 250 ng of pBR322 with increasing concentrations of PflAlba6 (0.25 μg, 0.5 μg, 1 μg, 1.5 μg, 2 μg, 2.5 μg, 5 μg respectively). Representative images from three technical replicates are shown.

a dose of artemisinin that reduced the parasite load by 50%, as seen through Giemsa staining of the control and the treated set (IC₅₀: 4 nM for 48 h) (Figures 9A and 9B). Real-Time quantitative PCR revealed that artemisinin induced a time-dependent increase of PflAlba6 mRNA compared to the control (Figure 9C). Further, exposing the parasites to heat stress at 39°C for 6 h induced a 4.7 ± 1-fold increase of the positive control PfHSP 70-x (Figure 9D) and a 10 ± 2-fold increase of PflAlba6 mRNA (Figure 9E) that returned to normal after a recovery period of 10 h at 37°C (Figures 9D and 9E). This indicates that PflAlba6 might play an important role in the parasite's homeostasis response.

DISCUSSION

We have extensively characterized PflAlba6-DNA interaction along with the oligomeric nature of this protein in the presence of DNA and the DNase activity of PflAlba6. The highly purified PflAlba6 is subjected to evaluate DNA binding and the consequent effect. PflAlba6 binds DNA

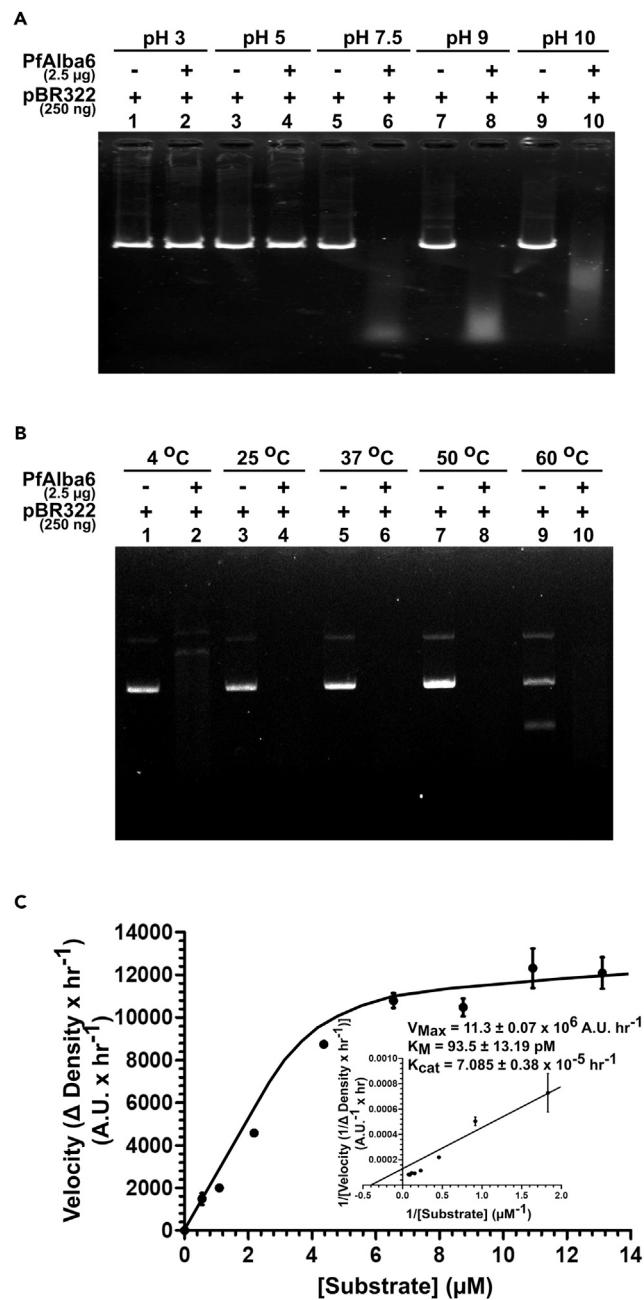


Figure 6. Nuclease activity of PfAlba6 across a wide range of temperatures and pH

(A) pH dependency on DNase activity of PfAlba6. DNase activity of PfAlba6 was carried out in different pH (3, 5, 7.5, 9, 10). (–) indicates control plasmid (250 ng of pBR322 in the respective pH buffers). (+) indicates the DNase activity of 250 ng of pBR322 with 2.5 μg PfAlba6 at different pH buffers. Representative images from three technical replicates are shown.

(B) Temperature - dependency on DNase activity of PfAlba6. DNase activity of PfAlba6 was carried out at different temperatures (4°C, 25°C, 37°C, 50°C, 60°C). (–) indicates control plasmid (250 ng of pBR322 at the respective pH buffers). (+) indicates the DNase activity of 250 ng of pBR322 with 2.5 μg PfAlba6 at different pH buffers. Representative images from three technical replicates are shown.

(C) Nuclease activity of PfAlba6 (2.5 μg) at different C28 DNA concentrations (0.15 μM, 0.3 μM, 0.6 μM, 1.2 μM, 1.8 μM, 2.4 μM, 3 μM, 3.6 μM) to calculate kinetic parameters by following Lineweaver-Burk plot (inset). Representative images from three technical replicates are shown.

sequence non-specifically with a high affinity, where binding of the DNA to the protein favors oligomerization of PfAlba6 at higher concentrations that was further confirmed by the volumetric analysis in size exclusion chromatography and single molecular imaging using atomic force microscopy of PfAlba6 in the absence and presence of DNA. To substantiate the above finding, we did single-molecule imaging in

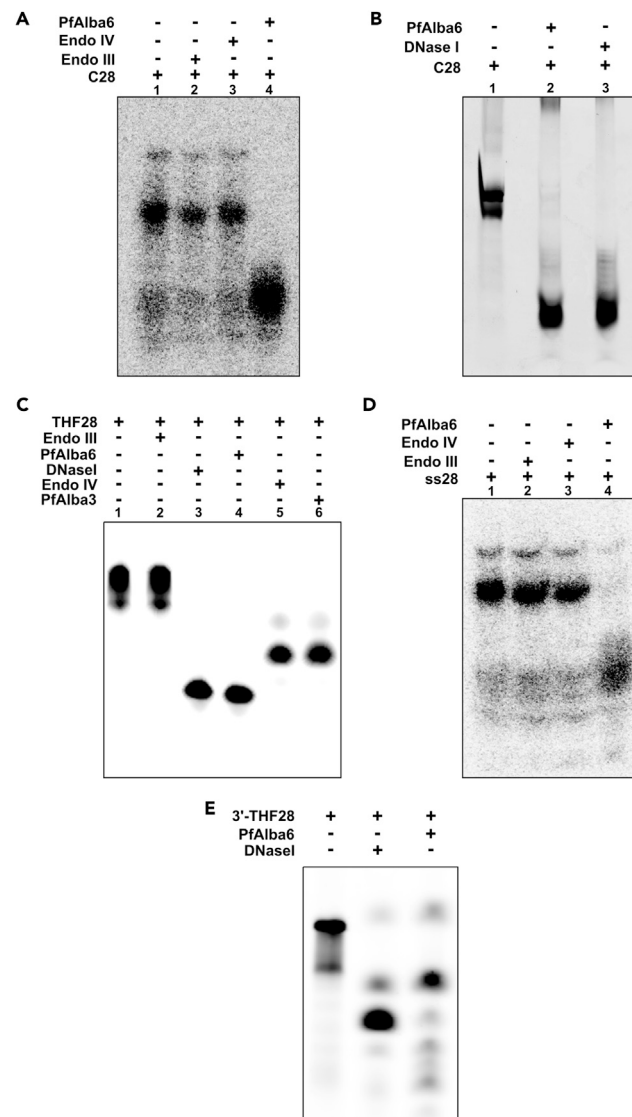


Figure 7. Determining the mechanism of DNase activity of PfAlba6

(A) Comparison of DNase activity of PfAlba6 with Endo III and Endo IV using radioactivity. Representative images from three technical replicates are shown. Lane 1: Control DNA (C28) (5'-labelled 28bp DNA with no abasic site in the presence of DNase buffer). Lane 2 and 3: C28 with 3 units of Endo III and Endo IV in their respective buffer. Lane 4: C28 with 2.5 μ g of PfAlba6.

(B) Comparison of DNase activity of PfAlba6 with DNase I using fluorescence. Lane 1: Control DNA (C28) (5'-FAM labeled 28bp DNA with no abasic site in the presence of DNase buffer). Lane 2: C28 with 2.5 μ g of PfAlba6. Lane 3: C28 with 3 units of DNase I. Representative images from three technical replicates are shown.

(C) Comparison of endonuclease activity of Endo III, DNase I, PfAlba6, Endo IV and PfAlba3 using fluorescence. Representative images from three technical replicates are shown. Lane 1: THF control DNA (THF28) (5'-FAM labeled 28bp DNA with THF at the 14th position mimicking an abasic site that can undergo hydroxylase activity with DNase buffer). Lane 2: THF28 has 3 units of Endo III in its respective buffer. Lane 3: THF28 with 3 units of DNase I in its respective buffer. Lane 4: THF28 with 2.5 μ g of PfAlba6 in the presence of its DNase buffer. Lane 5: THF28 with 3 units of Endo IV in its respective buffer. Lane 6: THF28 with 5 μ g of PfAlba3 in the presence of its DNase buffer (D) PfAlba6 can cleave ssDNA. Representative images from three technical replicates are shown. Lane 1: Control DNA (5' labeled 28bp ssDNA with DNase buffer). Lane 2 and 3: ssDNA with 3 units of Endo III and Endo IV in their respective buffer. Lane 4: ssDNA with 2.5 μ g of PfAlba6.

(E) Directionality of DNase activity of PfAlba6 using fluorescence. Lane 1: Control DNA (3'-C28) (3'-FAM labeled 28bp DNA with no abasic site in the presence of DNase buffer). Lane 2: 3'-C28 with 3 units of DNase I. Lane 3: 3'-C28 with 2.5 μ g of PfAlba6. Representative images from three technical replicates are shown.

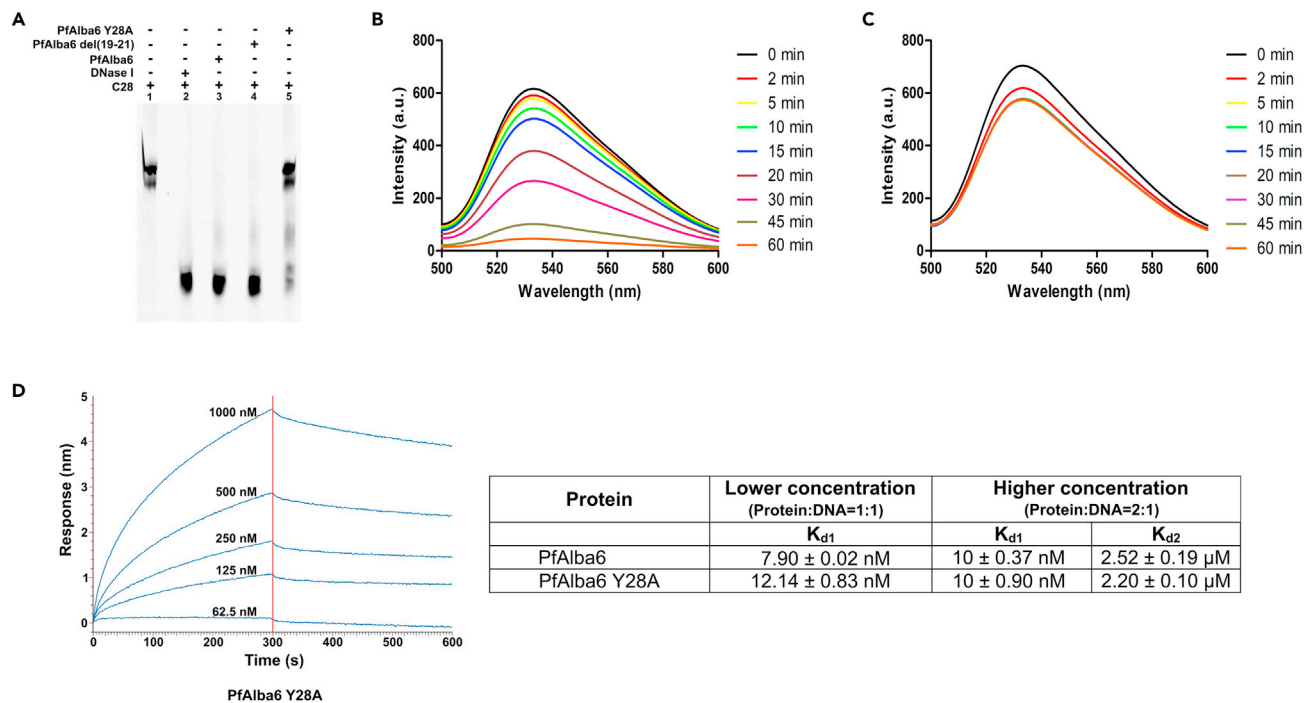


Figure 8. Determination of the residues involved in the DNase activity of PfAlba6

(A) Comparison of DNase activity of PfAlba6 with its mutated variants using fluorescence. Representative images from three technical replicates are shown. Lane 1: Control DNA (C28) (5'- FAM labeled 28bp DNA with no abasic site in DNase buffer). Lane 2: C28 with 3 units of DNase I. Lane 3: C28 with 2.5 μg of PfAlba6. Lane 4: C28 with 2.5 μg of PfAlba6 del (19–21). Lane 5: C28 with 2.5 μg of PfAlba6 Y28A. (B and C) Fluorometric analysis of real-time DNase activity of PfAlba6 and PfAlba6 Y28A by picogreen using 100 nM 28bp control DNA (C28) and 2.5 μg of PfAlba6 (B) and PfAlba6 Y28A (C). Representative images from three technical replicates are shown. (D) Biolayer Interferometry (BLI) analysis of the PfAlba6 Y28A –DNA interaction. 5 different concentrations of PfAlba6 Y28A (62.5 nM, 125 nM, 250 nM, 500 nM, 1000 nM) were subjected to BLI analysis. BLI was performed at 25°C in the BLI-buffer (25 mM Tris, 50 mM NaCl, pH: 7.5). A 28bp biotinylated dsDNA (44 μg/mL) was immobilized onto streptavidin-coated biosensor as the bait. The graphs show the association step for the first 300 s, and then the sensors were transferred to buffer-containing wells to measure dissociation (inset) Comparison of the K_d values for the interaction of the DNA with PfAlba6 and PfAlba6 Y28A as obtained from BLI. Representative images from three technical replicates are shown. Data are represented as mean ± SEM. See also Figure S2 and Table S4.

atomic force microscopy, intending to visualize the oligomeric nature of the protein morphologically by following an increase in the volume of PfAlba6 in the presence of DNA. AFM data clearly showed strong condensed complexes that harbor the formation of significant protein aggregation, which may be due to the cooperative nature of interaction.^{60,61} The binding of pBR322 by PfAlba6 causes strong condensation of the plasmid, forming large complexes with vertical dimensions between 2 and 3 nm. The clustering of PfAlba6 upon interacting with DNA may serve as the nucleation site, favoring oligomer formation.⁶² While characterizing the binding property of the protein in the presence of the metal ions, we observed it exhibits a 5' → 3' DNase activity in the presence of Mg^{2+} that is active in a wide range of temperature and pH (7.5–10), but different from DNase I. Although it is not uncommon for a nuclease to be active for a wide range of temperature and pH (such as RNaseA), the exact reason for PfAlba6 is not known. This may be attributed to the evolutionary conserved nature of the alba domain across all the species. The interaction of the protein and a metal ion can be a nonspecific electrostatic interaction, and a specific coordination bond formed either directly with the protein or with another ligand bound to the protein.⁶³ As can be seen, PfAlba6 also shows partial DNase activity in the presence of Mn^{2+} . Both Mg^{2+} and Mn^{2+} favor a “beta strand-binder-random coil” motif that acts as an active binder for them. While both the ions form coordination spheres that involve Asp and Gln, in the case of Mg^{2+} binding, His residue is under expressed, and in the case of Mn^{2+} , it is overexpressed. Mn^{2+} can substitute Mg^{2+} ions in the active sites of numerous enzymes.⁶³

PfAlba6, like PfAlba3, may be present in the acetylated form that has a lower affinity toward the DNA and thus its activity,⁴⁸ or like human DNases, may have another protein attached to PfAlba6 as a self-protection mechanism against premature DNA degradation.⁶⁴ PfAlba3 shows an abasic site-driven nuclease activity of dsDNA only. However, data indicated that PfAlba6 can target both dsDNA and ssDNA independent of the presence of any abasic site. This ability to cleave ssDNA coupled with its cytoplasmic distribution makes PfAlba6, like other PfAlbas, a potential RNA binding candidate having an RNase activity which calls for further investigations to understand its biological significance in the parasite. These data clearly suggests that different Albas may target different DNAs as substrates for DNA metabolism, which warrants further studies, as evidenced by the increased volume of the interacted protein PfAlba6.

PfAlba6 modeling by I-TASSER further predicted that specific residues are important in binding of the protein to the DNA. Based on those predictions, mutational studies revealed that tyrosine28 caused PfAlba6 to lose its activity. Tyrosine residues are known to play important

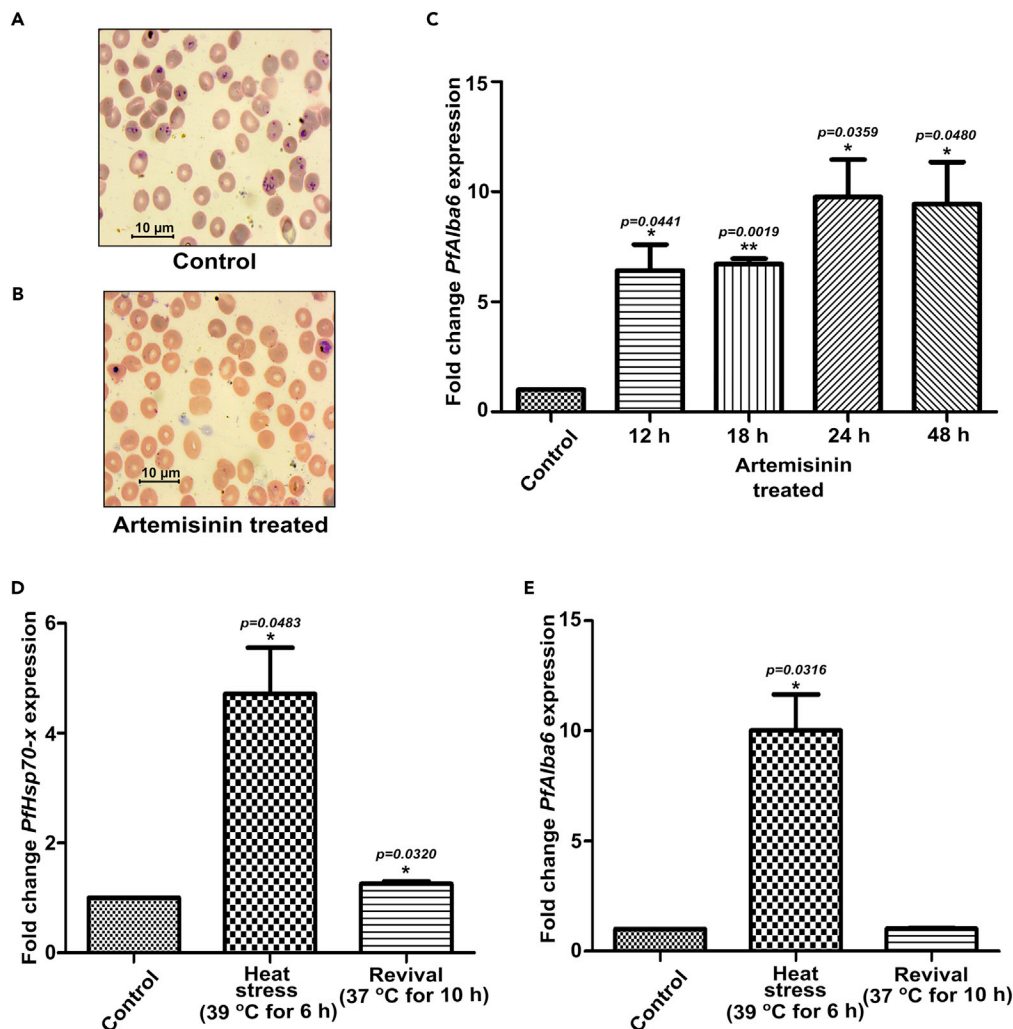


Figure 9. Effect of Artemisinin and heat on *PfAlba6* expression

(A and B) Giemsa stain of the intra-erythrocytic stages of *Plasmodium falciparum* in control (A) and 4 nM of artemisinin-treated (B) sets (48 h). Representative images from three technical replicates are shown.

(C) Differential expression profile of *PfAlba6* followed by Real-time PCR. A fold change of the gene was calculated between the control and artemisinin-treated *P. falciparum* parasite RNA in a time-dependent manner where *PfActinII* (Pf3D7_1412500) was used as reference control.

(D) Differential expression profile of *PfHsp70x* (Pf3D7_0831700) followed by Real-time PCR. A fold change of the gene was calculated between the control and heat-treated and revived *P. falciparum* parasite RNA, where *PfActinII* (Pf3D7_1412500) was used as reference control.

(E) Differential expression profile of *PfAlba6* followed by Real-time PCR. A fold change of the gene expression was calculated between the control and heat-treated and revived *P. falciparum* parasite RNA, where *PfActinII* (Pf3D7_1412500) was used as reference control. Statistical analysis has been performed using a two-tailed paired t-test, where p value represent * < 0.05; ** < 0.01. Data are represented as mean \pm SEM. n = 4 biological replicates.

roles in human AP Endonuclease I where mutation of the Tyr 171 leads to the protein inactivation, thus proposing the role of the residue in the rate-limiting catalytic step, even possibly acting as the attacking nucleophile itself.⁶⁵ The co-crystal structure revealed that this residue may be responsible for recognizing the abasic site in the DNA.⁶⁶ Tyrosine residues, present as a part of a nuclease's active sites, are also involved in DNA binding by forming stacking interactions with a base or a sugar moiety of the nucleic acid.⁶⁷ DNase I tyrosine76 plays an important role as a critical binding residue by forming a stacking interaction with the deoxyribose essential for phosphodiester bond cleavage.⁶⁸⁻⁷¹ However, mutation to the tyrosine28 in the *PfAlba6* did not hamper the DNA binding property of the protein, as is evident from the BLI. The exact mechanism of the DNase activity of the *PfAlba6* involving tyrosine28 residue could not be deciphered in the current study.

It was necessary to knock out the protein to understand its biological significance. However, *PfAlba6* has been regarded as an essential protein as it had not been successfully mutated using transposon mutagenesis of *P. falciparum*.⁷² Further, it has been shown that the essential genes may be important candidates responsible for drug resistance and represent leading vaccine candidates.⁷² Therefore, to elucidate the biological significance of this protein, we tried to determine its fate during stress. Alba proteins are known to play an essential role in

managing stress.⁷³ In *Arabidopsis*, Alba proteins are involved in heat response.⁷⁴ The Alba genes in tomato (*Solanum lycopersicum* L.), *Oryza sativa*, and cotton plants (*Gossypium hirsutum*) are known to play important roles in stress response.^{75,76} γ -irradiation interacts directly with the DNA, inducing oxidative stress by either repairable or irreparable DNA damages.^{77,78} γ -irradiation to *Plasmodium falciparum* saw a 7.19 ± 1.74 -fold upregulation of *PfAlba3* gene.^{48,79}

First-line anti-malarial drug, artemisinin (ART), is known to cause oxidative stress in parasites¹² by instigating genome instability due to the formation of ROS, which culminates to apoptosis-like death.^{9–11} Moreover, ART treatment induces growth retardation and an accumulation of ubiquitinated proteins⁵⁸ that leads to ER stress in the parasites.⁵⁹ Nucleases are known to play an important role in managing stress.¹⁵ During oxidative stress, the cleavage of tRNA required for protein synthesis is performed by an unknown endonuclease in *Plasmodium*, leading to increased gametocyte production.⁸⁰ Nucleases are known to play important roles in the DNA damage repair of the parasite as well.¹⁵ PfTatD, a *P. falciparum* TatD-like DNase, is a virulence factor expressed exclusively in the asexual blood stage of the parasite and is used by the parasite as a defense mechanism against neutrophil extracellular traps (NETs), composed primarily of DNA and proteases, which are released from activated neutrophils contributing to the innate immune response by capturing pathogens.⁸¹ Management of stress by malaria parasites is an exciting area for finding new drug targets. *Plasmodium* sp. has its defense tactics to prevent oxidative stress. In *P. falciparum*, thioredoxin and glutathione systems have been shown to play an important role in the defense mechanism against oxidative stress.⁸²

As *Plasmodium* sp. is sensitive to oxidative and heat stresses, targeting drugs against the proteins responsible for managing the parasite's stress can be a rationale for developing new antimalarial drugs. Moreover, periodic fever is the characteristic symptom of the malarial disease, during which the body temperature can reach $>40^{\circ}\text{C}$.⁸³ This thermal stress can kill parasite blood stages by programmed cell death pathways. To protect cells from heat stress, all organisms undergo several transcriptional changes. Thus, to determine the fate of this protein in artemisinin-induced oxidative stress and heat-induced stress of the parasite, it was found that the *PfAlba6* gene was upregulated by about 10-fold on the treatment of the parasite with artemisinin, which buttresses the role of this protein in oxidative stress response of the parasite. Further, the up-regulation of the gene upon heat stress by 10-fold validates that this protein might have an important role in stress response. However, the translational expression of this protein could not be determined because of our inability to get the protein through immunoblot due to the presence of the large amount of hemoglobin that masks the protein owing to the similar size of the subunits.

PfAlba6 is ubiquitously expressed in all the intra-erythrocytic stages of the parasites and may serve as a promising target. Although *P. falciparum* houses ten DNA endonucleases that may have various biological impact in the development of the parasite in the erythrocyte,⁸⁴ proteins involved in the management of stress in *P. falciparum* have not yet been targeted for the development of anti-malarials. Hence, this study advocates new directions for understanding the development of antimalarials by studying proteins involved in the stress management of *P. falciparum* and generating new antimalarials. Thus, if we could manipulate these targets by designing small molecules interacting with this protein, the parasite may be killed in other ways. So, this protein with no human orthologs may serve as an essential drug target.

Limitations of the study

The current study characterizes PfAlba6, an Alba domain protein from *P. falciparum*. We have shown that PfAlba6 binds DNA with high affinity forming higher order oligomeric complexes orchestrated by cooperative binding. Further we have shown that PfAlba6 exhibits Mg²⁺ dependent DNase activity cleaving both dsDNA and ssDNA in the 5'-3' polarity. The current study has some limitations. We were unable to determine whether PfAlba6 has any base or sequence preference for exerting its DNase activity. Although, immunofluorescence studies show PfAlba6 is housed both in cytoplasm as well as nucleus, more experimental evidence is required to verify its localization within the parasite. The cytoplasmic location of PfAlba6 coupled with its ability to cleave the ssDNA indicates the possibility of PfAlba6 to target and cleave RNA. It has been shown that tyrosine28 plays an important role in exhibiting DNase activity of the protein. But the precise role of this tyrosine remains elusive. The mRNA up-regulation of PfAlba6 in response to artemisinin and heat-induced stress suggest its role in the management of stress. However, we failed to provide the explicit molecular mechanism of the involvement of PfAlba6 in the management of stress in parasite. Furthermore, it remains to be explored whether PfAlba6 works alone or in sync with other Alba domain proteins. Since Alba domain are known to be modulated by acetylation deacetylation, how this PTM will impact PfAlba6 remains to be explored.

STAR★METHODS

Detailed methods are provided in the online version of this paper and include the following:

- KEY RESOURCES TABLE
- RESOURCE AVAILABILITY
 - Lead contact
 - Materials availability
 - Data and code availability
- EXPERIMENTAL MODEL AND STUDY PARTICIPANT DETAILS
 - Parasite strain
- METHOD DETAILS
 - Molecular modeling of PfAlba6
 - Parasite culture, synchronization and separation of parasite from infected erythrocytes
 - Extraction of RNA from parasite, cDNA preparation and PCR amplification

- Real-time PCR
- Cloning, overexpression and purification of PfAlba6
- Matrix-Assisted Laser Desorption/Ionization- time of Flight (MALDI-TOF) mass spectroscopy
- Circular dichroism spectroscopy
- Antibody generation
- Immunofluorescence assay
- Agarose gel shift assay
- Bio-layer interferometry (BLI)
- Atomic force microscopy (AFM)
- DNase activity of PfAlba6
- Metal ion - Dependency on the DNase activity of PfAlba6
- pH - Dependency on DNase activity of PfAlba6
- Temperature-dependency on DNase activity of PfAlba6
- Mutation of PfAlba6
- Autoradiography and fluorography
- Real-time assay of DNase activity
- **QUANTIFICATION AND STATISTICAL ANALYSIS**

SUPPLEMENTAL INFORMATION

Supplemental information can be found online at <https://doi.org/10.1016/j.isci.2024.109467>.

ACKNOWLEDGMENTS

We thank Mr. K. Suresh Kumar, Mr. Sounak Bhattacharyya, Mr. T. Muruganandan, and Mr. Sandip Chakraborty from the Central Instrumentation of Indian Institute of Chemical Biology (CSIR-IICB) for providing technical advice and assistance during the use of various instruments. We would like to specially thank Prof. (Dr.) Vishal Trivedi and Siddharth Neog from IIT Guwahati for his immense help for providing *P. falciparum*. We thank the Government of India for funding this research through the Council of Scientific & Industrial Research (CSIR) and providing a fellowship to S.N., C.B. through the University Grants Commission (UGC). U.B. would like to acknowledge J.C. Bose National Fellowship (Department of Science and Technology, Govt. of India; Grant No.: SB/S2/JCB-54/2014) for financial support.

AUTHOR CONTRIBUTIONS

Conceptualization, methodology, and writing, S.N. and U.B.; formal analysis, investigation and visualization, S.N., C.B., M.G., A.A.S., D.S., S.M., S.D., S.P., S.J.S., and R.D.; validation, supervision, project administration, and funding acquisition, U.B.

DECLARATION OF INTERESTS

The authors declare no competing interests.

Received: June 14, 2023

Revised: December 12, 2023

Accepted: March 7, 2024

Published: March 8, 2024

REFERENCES

1. Haque, U., Overgaard, H.J., Clements, A.C.A., Norris, D.E., Islam, N., Karim, J., Roy, S., Haque, W., Kabir, M., Smith, D.L., and Glass, G.E. (2014). Malaria burden and control in Bangladesh and prospects for elimination: an epidemiological and economic assessment. *Lancet. Glob. Health* 2, e98–e105. [https://doi.org/10.1016/S2214-109X\(13\)70176-1](https://doi.org/10.1016/S2214-109X(13)70176-1).
2. World malaria report (2019). <https://www.who.int/publications-detail-redirect/9789241565721>.
3. Woodrow, C.J., and White, N.J. (2017). The clinical impact of artemisinin resistance in Southeast Asia and the potential for future spread. *FEMS Microbiol. Rev.* 41, 34–48. <https://doi.org/10.1093/femsre/fuw037>.
4. Menard, D., and Dondorp, A. (2017). Antimalarial Drug Resistance: A Threat to Malaria Elimination. *Cold Spring Harb. Perspect. Med.* 7, a025619. <https://doi.org/10.1101/cshperspect.a025619>.
5. Ashley, E.A., Dhorda, M., Fairhurst, R.M., Amaratunga, C., Lim, P., Suon, S., Sreng, S., Anderson, J.M., Mao, S., Sam, B., et al. (2014). Spread of artemisinin resistance in *Plasmodium falciparum* malaria. *N. Engl. J. Med.* 371, 411–423. <https://doi.org/10.1056/NEJMoa1314981>.
6. Wongsrichanalai, C., and Sibley, C.H. (2013). Fighting drug-resistant *Plasmodium falciparum*: the challenge of artemisinin resistance. *Clin. Microbiol. Infect.* 19, 908–916. <https://doi.org/10.1111/1469-0691.12316>.
7. World Malaria Day: WHO identifies 25 countries with potential to be malaria-free by 2025 <https://www.downtoearth.org/in/news/africa/world-malaria-day-who-identifies-25-countries-with-potential-to-be-malaria-free-by-2025-76646>.
8. Sinha, S., Medhi, B., and Sehgal, R. (2014). Challenges of drug-resistant malaria. *Parasite* 21, 61. <https://doi.org/10.1051/parasite/2014059>.
9. Gupta, D.K., Patra, A.T., Zhu, L., Gupta, A.P., and Bozdech, Z. (2016). DNA damage regulation and its role in drug-related phenotypes in the malaria parasites. *Sci. Rep.* 6, 23603. <https://doi.org/10.1038/srep23603>.
10. Gunjan, S., Singh, S.K., Sharma, T., Dwivedi, H., Chauhan, B.S., Imran Siddiqi, M., and

- Tripathi, R. (2016). Mefloquine induces ROS mediated programmed cell death in malaria parasite: *Plasmodium*. *Apoptosis* 21, 955–964. <https://doi.org/10.1007/s10495-016-1265-y>.
11. Gopalakrishnan, A.M., and Kumar, N. (2015). Antimalarial action of artesunate involves DNA damage mediated by reactive oxygen species. *Antimicrob. Agents Chemother.* 59, 317–325. <https://doi.org/10.1128/AAC.03663-14>.
 12. Kavishv, R.A., Koenderink, J.B., and Alifrangis, M. (2017). Oxidative stress in malaria and artemisinin combination therapy: Pros and Cons. *FEBS J.* 284, 2579–2591. <https://doi.org/10.1111/febs.14097>.
 13. Kirkman, L.A., Lawrence, E.A., and Deitsch, K.W. (2014). Malaria parasites utilize both homologous recombination and alternative end joining pathways to maintain genome integrity. *Nucleic Acids Res.* 42, 370–379. <https://doi.org/10.1093/nar/gkt881>.
 14. Badugu, S.B., Nabi, S.A., Vaidyam, P., Laskar, S., Bhattacharyya, S., and Bhattacharyya, M.K. (2015). Identification of Plasmodium falciparum DNA Repair Protein Mre11 with an Evolutionarily Conserved Nuclease Function. *PLoS One* 10, e0125358. <https://doi.org/10.1371/journal.pone.0125358>.
 15. Lee, A.H., Symington, L.S., and Fidock, D.A. (2014). DNA repair mechanisms and their biological roles in the malaria parasite *Plasmodium falciparum*. *Microbiol. Mol. Biol. Rev.* 78, 469–486. <https://doi.org/10.1128/MMBR.00059-13>.
 16. Weber, J.L. (1987). Analysis of sequences from the extremely A + T-rich genome of *Plasmodium falciparum*. *Gene* 52, 103–109. [https://doi.org/10.1016/0378-1119\(87\)90399-4](https://doi.org/10.1016/0378-1119(87)90399-4).
 17. Gardner, M.J., Hall, N., Fung, E., White, O., Berriman, M., Hyman, R.W., Carlton, J.M., Pain, A., Nelson, K.E., Bowman, S., et al. (2002). Genome sequence of the human malaria parasite *Plasmodium falciparum*. *Nature* 419, 498–511. <https://doi.org/10.1038/nature01097>.
 18. Hall, N., Pain, A., Berriman, M., Churcher, C., Harris, B., Harris, D., Mungall, K., Bowman, S., Atkin, R., Baker, S., et al. (2002). Sequence of *Plasmodium falciparum* chromosomes 1, 3-9 and 13. *Nature* 419, 527–531. <https://doi.org/10.1038/nature01095>.
 19. Claessens, A., Harris, L.M., Stanojic, S., Chappell, L., Stanton, A., Kuk, N., Veneziano-Broccia, P., Sterkers, Y., Rayner, J.C., and Merrick, C.J. (2018). RecQ helicases in the malaria parasite *Plasmodium falciparum* affect genome stability, gene expression patterns and DNA replication dynamics. *PLoS Genet.* 14, e1007490. <https://doi.org/10.1371/journal.pgen.1007490>.
 20. Silberhorn, E., Schwartz, U., Löffler, P., Schmitz, S., Symelka, A., de Koning-Ward, T., Merkl, R., and Längst, G. (2016). *Plasmodium falciparum* Nucleosomes Exhibit Reduced Stability and Lost Sequence Dependent Nucleosome Positioning. *PLoS Pathog.* 12, e1006080. <https://doi.org/10.1371/journal.ppat.1006080>.
 21. Cui, L., Fan, Q., and Li, J. (2002). The malaria parasite *Plasmodium falciparum* encodes members of the Puf RNA-binding protein family with conserved RNA binding activity. *Nucleic Acids Res.* 30, 4607–4617. <https://doi.org/10.1093/nar/gkf600>.
 22. De Silva, E.K., Gehrke, A.R., Olszewski, K., León, I., Chahal, J.S., Bulyk, M.L., and Llinás, M. (2008). Specific DNA-binding by apicomplexan AP2 transcription factors. *Proc. Natl. Acad. Sci. USA* 105, 8393–8398. <https://doi.org/10.1073/pnas.0801993105>.
 23. Gissot, M., Briquet, S., Refour, P., Boschet, C., and Vaquero, C. (2005). PFMb1, a *Plasmodium falciparum* transcription factor, is required for intra-erythrocytic growth and controls key genes for cell cycle regulation. *J. Mol. Biol.* 346, 29–42. <https://doi.org/10.1016/j.jmb.2004.11.045>.
 24. Kumar, K., Singal, A., Rizvi, M.M.A., and Chauhan, V.S. (2008). High mobility group box (HMGB) proteins of *Plasmodium falciparum*: DNA binding proteins with pro-inflammatory activity. *Parasitol. Int.* 57, 150–157. <https://doi.org/10.1016/j.parint.2007.11.005>.
 25. Mancio-Silva, L., Rojas-Meza, A.P., Vargas, M., Scherf, A., and Hernandez-Rivas, R. (2008). Differential association of Orc1 and Sir2 proteins to telomeric domains in *Plasmodium falciparum*. *J. Cell Sci.* 121, 2046–2053. <https://doi.org/10.1242/jcs.026427>.
 26. McAndrew, M.B., Read, M., Sims, P.F., and Hyde, J.E. (1993). Characterisation of the gene encoding an unusually divergent TATA-binding protein (TBP) from the extremely A+T-rich human malaria parasite *Plasmodium falciparum*. *Gene* 124, 165–171. [https://doi.org/10.1016/0378-1119\(93\)90390-o](https://doi.org/10.1016/0378-1119(93)90390-o).
 27. Merrick, C.J., and Duraisingh, M.T. (2007). *Plasmodium falciparum* Sir2: an unusual sirtuin with dual histone deacetylase and ADP-ribosyltransferase activity. *Eukaryot. Cell* 6, 2081–2091. <https://doi.org/10.1128/EC.00114-07>.
 28. Bell, S.D., Botting, C.H., Wardleworth, B.N., Jackson, S.P., and White, M.F. (2002). The interaction of Alba, a conserved archaeal chromatin protein, with Sir2 and its regulation by acetylation. *Science* 296, 148–151. <https://doi.org/10.1126/science.1070506>.
 29. Forterre, P., Confalonieri, F., and Knapp, S. (1999). Identification of the gene encoding archaeal-specific DNA-binding proteins of the Sac10b family. *Mol. Microbiol.* 32, 669–670. <https://doi.org/10.1046/j.1365-2958.1999.01366.x>.
 30. Xue, H., Guo, R., Wen, Y., Liu, D., and Huang, L. (2000). An abundant DNA binding protein from the hyperthermophilic archaeon *Sulfolobus shibatae* affects DNA supercoiling in a temperature-dependent fashion. *J. Bacteriol.* 182, 3929–3933. <https://doi.org/10.1128/JB.182.14.3929-3933.2000>.
 31. Wardleworth, B.N., Russell, R.J.M., Bell, S.D., Taylor, G.L., and White, M.F. (2002). Structure of Alba: an archaeal chromatin protein modulated by acetylation. *EMBO J.* 21, 4654–4662. <https://doi.org/10.1093/emboj/cdf465>.
 32. Marsh, V.L., Peak-Chew, S.Y., and Bell, S.D. (2005). Sir2 and the acetyltransferase, Pat, regulate the archaeal chromatin protein, Alba. *J. Biol. Chem.* 280, 21122–21128. <https://doi.org/10.1074/jbc.M501280200>.
 33. Starai, V.J., and Escalante-Semerena, J.C. (2004). Identification of the protein acetyltransferase (Pat) enzyme that acetylates acetyl-CoA synthetase in *Salmonella enterica*. *J. Mol. Biol.* 340, 1005–1012. <https://doi.org/10.1016/j.jmb.2004.05.010>.
 34. Allers, T., and Meverach, M. (2005). Archaeal genetics - the third way. *Nat. Rev. Genet.* 6, 58–73. <https://doi.org/10.1038/nrg1504>.
 35. Peeters, E., Driessen, R.P.C., Werner, F., and Dame, R.T. (2015). The interplay between nucleoid organization and transcription in archaeal genomes. *Nat. Rev. Microbiol.* 13, 333–341. <https://doi.org/10.1038/nrmicro3467>.
 36. Reeve, J.N. (2003). Archaeal chromatin and transcription. *Mol. Microbiol.* 48, 587–598. <https://doi.org/10.1046/j.1365-2958.2003.03439.x>.
 37. Aravind, L., Iyer, L.M., and Anantharaman, V. (2003). The two faces of Alba: the evolutionary connection between proteins participating in chromatin structure and RNA metabolism. *Genome Biol.* 4, R64. <https://doi.org/10.1186/gb-2003-4-10-r64>.
 38. Liu, Q., and Dreyfuss, G. (1995). In vivo and in vitro arginine methylation of RNA-binding proteins. *Mol. Cell Biol.* 15, 2800–2808. <https://doi.org/10.1128/MCB.15.5.2800>.
 39. Chène, A., Vembar, S.S., Rivière, L., Lopez-Rubio, J.J., Claes, A., Siegel, T.N., Sakamoto, H., Scheidig-Benatar, C., Hernandez-Rivas, R., and Scherf, A. (2012). PfAlbas constitute a new eukaryotic DNA/RNA-binding protein family in malaria parasites. *Nucleic Acids Res.* 40, 3066–3077. <https://doi.org/10.1093/nar/gkr1215>.
 40. Guo, L., Ding, J., Guo, R., Hou, Y., Wang, D.-C., and Huang, L. (2014). Biochemical and structural insights into RNA binding by Ssh10b, a member of the highly conserved Sac10b protein family in Archaea. *J. Biol. Chem.* 289, 1478–1490. <https://doi.org/10.1074/jbc.M113.521351>.
 41. Mani, J., Güttinger, A., Schimanski, B., Heller, M., Acosta-Serrano, A., Pescher, P., Späth, G., and Roditi, I. (2011). Alba-domain proteins of *Trypanosoma brucei* are cytoplasmic RNA-binding proteins that interact with the translation machinery. *PLoS One* 6, e22463. <https://doi.org/10.1371/journal.pone.0022463>.
 42. Subota, I., Rotureau, B., Blisnick, T., Ngwabyt, S., Durand-Dubief, M., Engstler, M., and Bastin, P. (2011). ALBA proteins are stage regulated during trypanosome development in the tsetse fly and participate in differentiation. *Mol. Biol. Cell* 22, 4205–4219. <https://doi.org/10.1091/mbc.E11-06-0511>.
 43. Ellis, J.C., Barnes, J., and Brown, J.W. (2007). Is Alba an RNase P subunit? *RNA Biol.* 4, 169–172. <https://doi.org/10.4161/rna.4.3.5347>.
 44. Guo, R., Xue, H., and Huang, L. (2003). Ssh10b, a conserved thermophilic archaeal protein, binds RNA in vivo. *Mol. Microbiol.* 50, 1605–1615. <https://doi.org/10.1046/j.1365-2958.2003.03793.x>.
 45. Verma, J.K., Gayali, S., Dass, S., Kumar, A., Parveen, S., Chakraborty, S., and Chakraborty, N. (2014). OsAlba1, a dehydration-responsive nuclear protein of rice (*Oryza sativa* L. ssp. indica), participates in stress adaptation. *Phytochemistry* 100, 16–25. <https://doi.org/10.1016/j.phytochem.2014.01.015>.
 46. Yuan, W., Zhou, J., Tong, J., Zhuo, W., Wang, L., Li, Y., Sun, Q., and Qian, W. (2019). ALBA protein complex reads genetic R-loops to maintain genome stability in Arabidopsis. *Sci. Adv.* 5, eaav9040. <https://doi.org/10.1126/sciadv.aav9040>.

47. Lurz, R., Grote, M., Dijk, J., Reinhardt, R., and Dobrinski, B. (1986). Electron microscopic study of DNA complexes with proteins from the Archaeobacterium *Sulfolobus acidocaldarius*. *EMBO J.* 5, 3715–3721. <https://doi.org/10.1002/j.1460-2075.1986.tb04705.x>.
48. Banerjee, C., Nag, S., Goyal, M., Saha, D., Siddiqui, A.A., Mazumder, S., Debsharma, S., Pramanik, S., and Bandyopadhyay, U. (2023). Nuclease activity of *Plasmodium falciparum* Alba family protein PfAlba3. *Cell Rep.* 42, 112292. <https://doi.org/10.1016/j.celrep.2023.112292>.
49. Goyal, M., Alam, A., Iqbal, M.S., Dey, S., Bindu, S., Pal, C., Banerjee, A., Chakrabarti, S., and Bandyopadhyay, U. (2012). Identification and molecular characterization of an Alba-family protein from human malaria parasite *Plasmodium falciparum*. *Nucleic Acids Res.* 40, 1174–1190. <https://doi.org/10.1093/nar/gkr821>.
50. Wang, S., Li, W., Liu, S., and Xu, J. (2016). RaptorX-Property: a web server for protein structure property prediction. *Nucleic Acids Res.* 44, W430–W435. <https://doi.org/10.1093/nar/gkw306>.
51. Wang, S., Ma, J., and Xu, J. (2016). AUCpreD: proteome-level protein disorder prediction by AUC-maximized deep convolutional neural fields. *Bioinformatics* 32, i672–i679. <https://doi.org/10.1093/bioinformatics/btw446>.
52. Wang, S., Sun, S., and Xu, J. (2016). AUC-Maximized Deep Convolutional Neural Fields for Protein Sequence Labeling. *Mach. Learn. Knowl. Discov. Databases.* 9852, 1–16. https://doi.org/10.1007/978-3-319-46227-1_1.
53. Wang, S., Peng, J., Ma, J., and Xu, J. (2016). Protein Secondary Structure Prediction Using Deep Convolutional Neural Fields. *Sci. Rep.* 6, 18962. <https://doi.org/10.1038/srep18962>.
54. Shepherd, N.E., Hoang, H.N., Abbenante, G., and Fairlie, D.P. (2005). Single turn peptide alpha helices with exceptional stability in water. *J. Am. Chem. Soc.* 127, 2974–2983. <https://doi.org/10.1021/ja0456003>.
55. Lau, S.Y., Taneja, A.K., and Hodges, R.S. (1984). Synthesis of a model protein of defined secondary and quaternary structure. Effect of chain length on the stabilization and formation of two-stranded alpha-helical coiled-coils. *J. Biol. Chem.* 259, 13253–13261.
56. Kwok, S.C., and Hodges, R.S. (2004). Stabilizing and destabilizing clusters in the hydrophobic core of long two-stranded alpha-helical coiled-coils. *J. Biol. Chem.* 279, 21576–21588. <https://doi.org/10.1074/jbc.M401074200>.
57. Crooks, R.O., Rao, T., and Mason, J.M. (2011). Truncation, randomization, and selection: generation of a reduced length c-Jun antagonist that retains high interaction stability. *J. Biol. Chem.* 286, 29470–29479. <https://doi.org/10.1074/jbc.M111.221267>.
58. Dogovski, C., Xie, S.C., Burgio, G., Bridgford, J., Mok, S., McCaw, J.M., Chotivanich, K., Kenny, S., Gnädig, N., Straimer, J., et al. (2015). Targeting the cell stress response of *Plasmodium falciparum* to overcome artemisinin resistance. *PLoS Biol.* 13, e1002132. <https://doi.org/10.1371/journal.pbio.1002132>.
59. Bridgford, J.L., Xie, S.C., Cobbold, S.A., Pasaje, C.F.A., Herrmann, S., Yang, T., Gillett, D.L., Dick, L.R., Ralph, S.A., Dogovski, C., et al. (2018). Artemisinin kills malaria parasites by damaging proteins and inhibiting the proteasome. *Nat. Commun.* 9, 3801. <https://doi.org/10.1038/s41467-018-06221-1>.
60. Peeters, E., Boon, M., Rollie, C., Willaert, R.G., Voet, M., White, M.F., Prangishvili, D., Lavigne, R., and Quax, T.E.F. (2017). DNA-Interacting Characteristics of the Archaeal Rudiviral Protein SIRV2_Gp1. *Viruses* 9, 190. <https://doi.org/10.3390/v9070190>.
61. van Noort, J., Verbrugge, S., Goosen, N., Dekker, C., and Dame, R.T. (2004). Dual architectural roles of HU: formation of flexible hinges and rigid filaments. *Proc. Natl. Acad. Sci. USA* 101, 6969–6974. <https://doi.org/10.1073/pnas.0308230101>.
62. Mohan Bangalore, D., and Tessmer, I. (2018). Unique insight into protein-DNA interactions from single molecule atomic force microscopy. *AIMS Biophys.* 5, 194–216. <https://doi.org/10.3934/biophys.2018.3.194>.
63. Khrustalev, V.V., Barkovskiy, E.V., and Khrustaleva, T.A. (2016). Magnesium and manganese binding sites on proteins have the same predominant motif of secondary structure. *J. Theor. Biol.* 395, 174–185. <https://doi.org/10.1016/j.jtbi.2016.02.006>.
64. Eulitz, D., and Mannherz, H.G. (2007). Inhibition of deoxyribonuclease I by actin is to protect cells from premature cell death. *Apoptosis* 12, 1511–1521. <https://doi.org/10.1007/s10495-007-0078-4>.
65. Mundle, S.T., Fattal, M.H., Melo, L.F., Coriolan, J.D., O'Regan, N.E., and Strauss, P.R. (2004). Novel role of tyrosine in catalysis by human AP endonuclease 1. *DNA Repair* 3, 1447–1455. <https://doi.org/10.1016/j.dnarep.2004.06.009>.
66. Mol, C.D., Izumi, T., Mitra, S., and Tainer, J.A. (2000). DNA-bound structures and mutants reveal abasic DNA binding by APE1 and DNA repair coordination [corrected]. *Nature* 403, 451–456. <https://doi.org/10.1038/35000249>.
67. Korn, C., Scholz, S.R., Gimadutdinov, O., Pingoud, A., and Meiss, G. (2002). Involvement of conserved histidine, lysine and tyrosine residues in the mechanism of DNA cleavage by the caspase-3 activated DNase CAD. *Nucleic Acids Res.* 30, 1325–1332. <https://doi.org/10.1093/nar/30.6.1325>.
68. Weston, S.A., Lahm, A., and Suck, D. (1992). X-ray structure of the DNase I-d(GGTATACC)₂ complex at 2.3 Å resolution. *J. Mol. Biol.* 226, 1237–1256. [https://doi.org/10.1016/0022-2836\(92\)91064-v](https://doi.org/10.1016/0022-2836(92)91064-v).
69. Doherty, A.J., Worrall, A.F., and Connolly, B.A. (1995). The roles of arginine 41 and tyrosine 76 in the coupling of DNA recognition to phosphodiester bond cleavage by DNase I: a study using site-directed mutagenesis. *J. Mol. Biol.* 251, 366–377. <https://doi.org/10.1006/jmbi.1995.0440>.
70. Warren, M.A., Evans, S.J., and Connolly, B.A. (1997). Effects of non-conservative changes to tyrosine 76, a key DNA binding residue of DNase I, on phosphodiester bond cleavage and DNA hydrolysis selectivity. *Protein Eng.* 10, 279–283. <https://doi.org/10.1093/protein/10.3.279>.
71. Pan, C.Q., Ulmer, J.S., Herzka, A., and Lazarus, R.A. (1998). Mutational analysis of human DNase I at the DNA binding interface: implications for DNA recognition, catalysis, and metal ion dependence. *Protein Sci.* 7, 628–636. <https://doi.org/10.1002/pro.5560070312>.
72. Zhang, M., Wang, C., Otto, T.D., Oberstaller, J., Liao, X., Adapa, S.R., Udenze, K., Bronner, I.F., Casandra, D., Mayho, M., et al. (2018). Uncovering the essential genes of the human malaria parasite *Plasmodium falciparum* by saturation mutagenesis. *Science* 360, eaap7847. <https://doi.org/10.1126/science.aap7847>.
73. Goyal, M., Banerjee, C., Nag, S., and Bandyopadhyay, U. (2016). The Alba protein family: Structure and function. *Biochim. Biophys. Acta* 1864, 570–583. <https://doi.org/10.1016/j.bbapap.2016.02.015>.
74. Náprstková, A., Malinská, K., Závěská Drábková, L., Billey, E., Náprstková, D., Šýkorová, E., Bousquet-Antonelli, C., and Honys, D. (2021). Characterization of ALBA Family Expression and Localization in *Arabidopsis thaliana* Generative Organs. *Int. J. Mol. Sci.* 22, 1652. <https://doi.org/10.3390/ijms22041652>.
75. Wai, A.H., Cho, L.-H., Peng, X., Waseem, M., Lee, D.-J., Lee, J.-M., Kim, C.-K., and Chung, M.-Y. (2021). Genome-wide identification and expression profiling of Alba gene family members in response to abiotic stress in tomato (*Solanum lycopersicum* L.). *BMC Plant Biol.* 21, 530. <https://doi.org/10.1186/s12870-021-03310-0>.
76. Verma, J.K., Wardhan, V., Singh, D., Chakraborty, S., and Chakraborty, N. (2018). Genome-Wide Identification of the Alba Gene Family in Plants and Stress-Responsive Expression of the Rice Alba Genes. *Genes* 9, 183. <https://doi.org/10.3390/genes9040183>.
77. Tsyusko, O., Yi, Y., Coughlin, D., Main, D., Podolsky, R., Hinton, T.G., and Glenn, T.C. (2007). Radiation-induced untargeted germline mutations in Japanese medaka. *Comp. Biochem. Physiol. C Toxicol. Pharmacol.* 145, 103–110. <https://doi.org/10.1016/j.cbpc.2006.08.010>.
78. Rhee, J.-S., Kim, B.-M., Kang, C.-M., Lee, Y.-M., and Lee, J.-S. (2012). Gamma irradiation-induced oxidative stress and developmental impairment in the hermaphroditic fish, *Kryptolebias marmoratus* embryo. *Environ. Toxicol. Chem.* 31, 1745–1753. <https://doi.org/10.1002/etc.1873>.
79. Oakley, M.S., Verma, N., Zheng, H., Anantharaman, V., Takeda, K., Gao, Y., Myers, T.G., Pham, P.T., Mahajan, B., Kumar, N., et al. (2016). Molecular Markers of Radiation Induced Attenuation in Intrahepatic *Plasmodium falciparum* Parasites. *PLoS One* 11, e0166814. <https://doi.org/10.1371/journal.pone.0166814>.
80. Hammam, E., Sinha, A., Baumgarten, S., Nardella, F., Liang, J., Miled, S., Bonhomme, F., Erdmann, D., Arcangioli, B., Arimondo, P.B., et al. (2021). Malaria Parasite Stress Tolerance Is Regulated by DNMT2-Mediated tRNA Cytosine Methylation. *mBio* 12, e0255821. <https://doi.org/10.1128/mBio.02558-21>.
81. Chang, Z., Jiang, N., Zhang, Y., Lu, H., Yin, J., Wahlgren, M., Cheng, X., Cao, Y., and Chen, Q. (2016). The TatD-like DNase of *Plasmodium* is a virulence factor and a potential malaria vaccine candidate. *Nat. Commun.* 7, 11537. <https://doi.org/10.1038/ncomms11537>.

82. Sahu, N.K., Sahu, S., and Kohli, D.V. (2008). Novel molecular targets for antimalarial drug development. *Chem. Biol. Drug Des.* 71, 287–297. <https://doi.org/10.1111/j.1747-0285.2008.00640.x>.
83. Tintó-Font, E., and Cortés, A. (2022). Malaria parasites do respond to heat. *Trends Parasitol.* 38, 435–449. <https://doi.org/10.1016/j.pt.2022.02.009>.
84. Jiang, N., Tu, Z., Zhang, Y., Li, J., Feng, Y., Yang, N., Sang, X., and Chen, Q. (2018). Identification and characterization of DNA endonucleases in *Plasmodium falciparum* 3D7 clone. *Malar. J.* 17, 232. <https://doi.org/10.1186/s12936-018-2388-0>.
85. Katoh, K., Kuma, K.I., Miyata, T., and Toh, H. (2005). Improvement in the accuracy of multiple sequence alignment program MAFFT. *Genome Inform.* 16, 22–33.
86. Waterhouse, A.M., Procter, J.B., Martin, D.M.A., Clamp, M., and Barton, G.J. (2009). Jalview Version 2—a multiple sequence alignment editor and analysis workbench. *Bioinformatics* 25, 1189–1191. <https://doi.org/10.1093/bioinformatics/btp033>.
87. Zhang, Y. (2009). I-TASSER: fully automated protein structure prediction in CASP8. *Proteins* 77 (Suppl 9), 100–113. <https://doi.org/10.1002/prot.22588>.
88. Yang, J., and Zhang, Y. (2015). I-TASSER server: new development for protein structure and function predictions. *Nucleic Acids Res.* 43, W174–W181. <https://doi.org/10.1093/nar/gkv342>.
89. Roy, A., Yang, J., and Zhang, Y. (2012). COFACTOR: an accurate comparative algorithm for structure-based protein function annotation. *Nucleic Acids Res.* 40, W471–W477. <https://doi.org/10.1093/nar/gks372>.
90. Mozumder, S., Bej, A., Srinivasan, K., Mukherjee, S., and Sengupta, J. (2020). Comprehensive structural modeling and preparation of human 5-HT2A G-protein coupled receptor in functionally active form. *Biopolymers* 111, e23329. <https://doi.org/10.1002/bip.23329>.
91. Lovell, S.C., Davis, I.W., Arendall, W.B., de Bakker, P.I.W., Word, J.M., Prisant, M.G., Richardson, J.S., and Richardson, D.C. (2003). Structure validation by Calpha geometry: phi,psi and Cbeta deviation. *Proteins* 50, 437–450. <https://doi.org/10.1002/prot.10286>.
92. Colovos, C., and Yeates, T.O. (1993). Verification of protein structures: patterns of nonbonded atomic interactions. *Protein Sci.* 2, 1511–1519. <https://doi.org/10.1002/pro.5560020916>.
93. Wiederstein, M., and Sippl, M.J. (2007). ProSA-web: interactive web service for the recognition of errors in three-dimensional structures of proteins. *Nucleic Acids Res.* 35, W407–W410. <https://doi.org/10.1093/nar/gkm290>.
94. Sippl, M.J. (1993). Recognition of errors in three-dimensional structures of proteins. *Proteins* 17, 355–362. <https://doi.org/10.1002/prot.340170404>.
95. Cristobal, S., Zemla, A., Fischer, D., Rychlewski, L., and Elofsson, A. (2001). A study of quality measures for protein threading models. *BMC Bioinf.* 2, 5. <https://doi.org/10.1186/1471-2105-2-5>.
96. Trager, W., and Jensen, J.B. (1976). Human malaria parasites in continuous culture. *Science* 193, 673–675. <https://doi.org/10.1126/science.781840>.
97. Sarkar, S., Siddiqui, A.A., Saha, S.J., De, R., Mazumder, S., Banerjee, C., Iqbal, M.S., Nag, S., Adhikari, S., and Bandyopadhyay, U. (2016). Antimalarial Activity of Small-Molecule Benzothiazole Hydrazones. *Antimicrob. Agents Chemother.* 60, 4217–4228. <https://doi.org/10.1128/AAC.01575-15>.
98. Theron, M., Cross, N., Cawkill, P., Bustamante, L.Y., and Rayner, J.C. (2018). An in vitro erythrocyte preference assay reveals that *Plasmodium falciparum* parasites prefer Type O over Type A erythrocytes. *Sci. Rep.* 8, 8133. <https://doi.org/10.1038/s41598-018-26559-2>.
99. Wallach, M. (1982). Efficient extraction and translation of *Plasmodium falciparum* messenger RNA. *Mol. Biochem. Parasitol.* 6, 335–342. [https://doi.org/10.1016/0166-6851\(82\)90023-8](https://doi.org/10.1016/0166-6851(82)90023-8).
100. Biswas, S., Saxena, Q.B., Roy, A., and Sharma, V.P. (1988). Isolation of different erythrocytic stages of *Plasmodium falciparum* and synchronization in culture. *Indian J. Malariol.* 25, 7–10.
101. Lambros, C., and Vanderberg, J.P. (1979). Synchronization of *Plasmodium falciparum* erythrocytic stages in culture. *J. Parasitol.* 65, 418–420.
102. Das, S., Banerjee, A., Kamran, M., Ejazi, S.A., Asad, M., Ali, N., and Chakrabarti, S. (2020). A chemical inhibitor of heat shock protein 78 (HSP78) from *Leishmania donovani* represents a potential antileishmanial drug candidate. *J. Biol. Chem.* 295, 9934–9947. <https://doi.org/10.1074/jbc.RA120.014587>.
103. Micsonai, A., Bulyáki, É., and Kardos, J. (2021). BeStSel: From Secondary Structure Analysis to Protein Fold Prediction by Circular Dichroism Spectroscopy. In *Structural Genomics Methods in Molecular Biology*, Y.W. Chen and C.-P.B. Yiu, eds. (Springer US), pp. 175–189. https://doi.org/10.1007/978-1-0716-0892-0_11.
104. Iqbal, M.S., Siddiqui, A.A., Alam, A., Goyal, M., Banerjee, C., Sarkar, S., Mazumder, S., De, R., Nag, S., Saha, S.J., and Bandyopadhyay, U. (2016). Expression, purification and characterization of *Plasmodium falciparum* vacuolar protein sorting 29. *Protein Expr. Purif.* 120, 7–15. <https://doi.org/10.1016/j.pep.2015.12.004>.
105. Dey, S., Mazumder, S., Siddiqui, A.A., Iqbal, M.S., Banerjee, C., Sarkar, S., De, R., Goyal, M., Bindu, S., and Bandyopadhyay, U. (2014). Association of heme oxygenase 1 with the restoration of liver function after damage in murine malaria by *Plasmodium yoelii*. *Infect. Immun.* 82, 3113–3126. <https://doi.org/10.1128/IAI.01598-14>.
106. Dey, S., Bindu, S., Goyal, M., Pal, C., Alam, A., Iqbal, M.S., Kumar, R., Sarkar, S., and Bandyopadhyay, U. (2019). Correction: Impact of intravascular hemolysis in malaria on liver dysfunction: Involvement of hepatic free heme overload, NF-κB activation, and neutrophil infiltration. *J. Biol. Chem.* 294, 20259. <https://doi.org/10.1074/jbc.AAC119.012033>.
107. Sultana, A., and Lee, J.E. (2015). Measuring protein-protein and protein-nucleic Acid interactions by biolayer interferometry. *Curr. Protoc. Protein Sci.* 79, 19–25. <https://doi.org/10.1002/0471140864.ps1925s79>.
108. Wang, X., Feng, Y., Bajaj, G., Gupta, M., Agrawal, S., Yang, A., Park, J.-S., Lestini, B., and Roy, A. (2017). Quantitative Characterization of the Exposure-Response Relationship for Cancer Immunotherapy: A Case Study of Nivolumab in Patients With Advanced Melanoma. *CPT Pharmacometrics Syst. Pharmacol.* 6, 40–48. <https://doi.org/10.1002/psp4.12133>.
109. Sharma, P., Tomar, A.K., and Kundu, B. (2018). Interplay between CedA, rpoB and double stranded DNA: A step towards understanding CedA mediated cell division in *E. coli*. *Int. J. Biol. Macromol.* 107, 2026–2033. <https://doi.org/10.1016/j.ijbiomac.2017.10.075>.
110. Ling, J., Liu, W.Y., and Wang, T.P. (1994). Cleavage of supercoiled double-stranded DNA by several ribosome-inactivating proteins in vitro. *FEBS Lett.* 345, 143–146. [https://doi.org/10.1016/0014-5793\(94\)00421-8](https://doi.org/10.1016/0014-5793(94)00421-8).
111. Nicolas, E., Beggs, J.M., Haltiwanger, B.M., and Taraschi, T.F. (1997). Direct evidence for the deoxyribonuclease activity of the plant ribosome inactivating protein gelonin. *FEBS Lett.* 406, 162–164. [https://doi.org/10.1016/s0014-5793\(97\)00267-6](https://doi.org/10.1016/s0014-5793(97)00267-6).
112. Day, P.J., Lord, J.M., and Roberts, L.M. (1998). The deoxyribonuclease activity attributed to ribosome-inactivating proteins is due to contamination. *Eur. J. Biochem.* 258, 540–545. <https://doi.org/10.1046/j.1432-1327.1998.2580540.x>.
113. Haltiwanger, B.M., Karpinich, N.O., and Taraschi, T.F. (2000). Characterization of class II apurinic/aprimidinic endonuclease activities in the human malaria parasite, *Plasmodium falciparum*. *Biochem. J.* 345, 85–89.
114. McCullough, A.K., Sanchez, A., Dodson, M.L., Marapaka, P., Taylor, J.S., and Lloyd, R.S. (2001). The reaction mechanism of DNA glycosylase/AP lyases at abasic sites. *Biochemistry* 40, 561–568. <https://doi.org/10.1021/bi002404+>.
115. Tolun, G., and Myers, R.S. (2003). A real-time DNase assay (ReDA) based on PicoGreen fluorescence. *Nucleic Acids Res.* 31, e111. <https://doi.org/10.1093/nar/gng111>.

STAR★METHODS

KEY RESOURCES TABLE

REAGENT or RESOURCE	SOURCE	IDENTIFIER
Antibodies		
Goat anti-Rabbit IgG (H + L) Highly Cross-Adsorbed Secondary Antibody, Alexa Fluor 647	Invitrogen	Catalog # A-21245; RRID: AB_2535813
Anti-PfAlba6 antibody	Lab generated	NA
Bacterial and virus strains		
<i>Plasmodium falciparum</i> 3D7	ATCC	MRA-102
DH5 α <i>E.coli</i>	ThermoFischer Scientific	Catalog #18258012;
Rosetta(DE3)pLysS <i>E.coli</i>	Novagen	Catalog #70956-M
Biological samples		
Rabbit (New Zealand White strain)	In-house breeding	N.A.
Human erythrocytes from healthy individual with O+ Blood group	In house	N.A.
Chemicals, peptides, and recombinant proteins		
7-Nitroindole-2-carboxylic acid	Sigma- Aldrich	Cat #C0496-10MG
pBR322	Thermo Scientific™	Cat #SD0041
Endonuclease III	New England Biolabs	Cat #M0268S
Endonuclease IV	New England Biolabs	Cat #M0304S
T4 Polynucleotide Kinase	New England Biolabs	Cat #M0201S
Cyanogen Bromide	Sisco Research Lab	Cat#65291
Lambda DNA	Thermo Scientific	Cat#SD0011
(3-Aminopropyl)triethoxysilane	Sigma- Aldrich	Cat#440140
Isopropanol	Sigma- Aldrich	Cat#I9516
Trifluoroacetic acid	Sigma- Aldrich	Cat#1.08178
Paraformaldehyde	Sigma- Aldrich	Cat#158127
Gluteraldehyde solution	Sigma- Aldrich	Cat#G5882
Sodium Borohydride	Sigma- Aldrich	Cat#215538
Acetyl coenzyme A sodium salt	Sigma- Aldrich	Cat#A2056
NAD+	Sigma- Aldrich	Cat# NAD100-RO Roche
Pyridoxal 5'-phosphate hydrate	Sigma- Aldrich	Cat# P9255
Sodium Cyanoborohydride	Sigma- Aldrich	Cat# 156159
Methoxyamine hydrochloride	Sigma- Aldrich	Cat#226904
N,N'-Dimethylethylenediamine	Sigma- Aldrich	Cat#D157805
1,4-Dithiothreitol	Sigma- Aldrich	Cat# DTT-RO Roche
Ethylenediaminetetraacetic acid	Sigma- Aldrich	Cat#EDS
Ethylene glycol-bis(2-aminoethylether)-N,N,N',N'-tetraacetic acid	Sigma- Aldrich	Cat#E3889
Aurintricarboxylic acid	Sigma- Aldrich	Cat#A1895
IPTG, dioxane-free	Thermo Scientific™	Cat# R0392
HEPES	Sigma- Aldrich	Cat# H3375
(3-Aminopropyl)triethoxysilane	Sigma- Aldrich	Cat# 440140

(Continued on next page)

Continued

REAGENT or RESOURCE	SOURCE	IDENTIFIER
Miller Luria Bertani Broth	Himedia	Cat#GM1245
Miller Luria Bertani Agar	Himedia	Cat#M1151
Tris base	Sigma- Aldrich	Cat#TRIS-RO
Sodium chloride	Sigma- Aldrich	Cat#S9888
Quant-iT PicoGreen dsDNA Reagent	Invitrogen™	Cat#P11495
PageRuler™ Prestained Protein Ladder, 10 to 180 kDa	Thermo Scientific™	Cat#26616
RPMI-1640	Merck	Cat#R4130
D-(+)-Glucose	Sigma- Aldrich	Cat#G8270
Sodium bicarbonate	Sigma- Aldrich	Cat#S6014
Gentamicin solution	Merck	Cat# G1397
Hypoxanthine	Sigma- Aldrich	Cat# H9636
AlbuMAX™ II Lipid-Rich BSA	Gibco™ ThermoFisher Scientific	Cat#11021029
ProLong™ Diamond Antifade Mountant with DAPI	Invitrogen™	Cat# P36962
SYBR™ Safe DNA Gel Stain	Invitrogen™	S33102

Critical commercial assays

HiTrap® SP Fast Flow	Cytiva	GE17-5157-01
HiTrap® Q Fast Flow	Cytiva	GE17-5156-01
HiLoad 16/600 Superdex 75 pg	Cytiva	GE 28-9893-33
QIAprep Spin Miniprep Kit	Qiagen	Cat. No./ID: 27104
SA Biosensors	FORTEBIO	Cat#18-5019

Software and algorithms

Software platform for life science LAS X Life Science	Leica Microsystems	N.A.
Octet data analysis 11.0 software	BLI	N.A.
PicoView-Setup-1-20.2	AFM (Agilent)	N.A.
FL solution 1.7	Hitachi Fluorescence Spectrophotometer F-7000	N.A.
Gen5 1.07 Microplate Reader and Imager Software	BioTek Plate Reader (Agilent)	N.A.
Unicom 6.4	GE Healthcare	N.A.
Inkscape-1.0-x64.exe	Inkscape's Contributors	N.A.
Prism 5	GraphPad Prism 5.0	N.A.
Adobe Photoshop CS6	Adope	N.A.
ImageQuant™ TL image analysis software v7.0	GE Typhoon Trio Imager Scanner Fluorescence Chemiluminescent	N.A.
Image Lab Touch 2.4 Software	ChemiDoc MP Imaging System	N.A.

RESOURCE AVAILABILITY

Lead contact

Further information and requests for resources and reagents should be directed to and will be fulfilled by the lead contact, Uday Bandyopadhyay (ubandyo_1964@yahoo.com).

Materials availability

This study did not generate new unique reagents.

Data and code availability

- Any additional information required to reanalyze the data reported in this paper is available from the [lead contact](#) upon request.
- This paper does not report original code.
- Any additional information required to reanalyze the data reported in this paper is available from the [lead contact](#) upon request.

EXPERIMENTAL MODEL AND STUDY PARTICIPANT DETAILS

Parasite strain

Plasmodium falciparum 3D7 was obtained from BEI Resources Web Portal of ATCC (MRA-102) (RRID: NCBITaxon_36329).

METHOD DETAILS

Molecular modeling of PfAlba6

Plasmodium falciparum Alba6 (PfAlba6-PF3D7_1202800), a 96 amino acids long putative DNA binding protein, is localized on chromosome 12 (gene location-Pf3D7_12_v4:160,716..61,225(+)) of parasite genome. NCBI Blast search identified the exclusive presence of this protein in *Plasmodium falciparum* with no human orthologs. Multiple sequence alignment of PfAlba6 with other organisms [*Plasmodium vivax* (*P. vivax*), *Plasmodium vivax* India VII (*P. vivax* India VII), *Plasmodium berghei* ANKA (*P. berghei* ANKA), *Plasmodium yoelii* (*P. yoelii*), *Plasmodium reichenowi* (*P. reichenowi*), *Plasmodium falciparum*_HB3 (*P. falciparum* HB3), *Plasmodium gaboni* (*P. gaboni*), *Plasmodium relictum* (*P. relictum*), *Plasmodium gallinaceum* (*P. gallinaceum*), *Plasmodium malariae* (*P. malariae*), *Plasmodium coatneyi* (*P. coatneyi*), *Hepaticystis* sp.] was performed by the MAFFT software⁸⁵ and explored by Jalview program.⁸⁶ Analysis of PfAlba6 amino acid sequence using <https://www.predictprotein.org/> identified an "alpha-beta" secondary structure with no non-ordinary secondary structures. The localization of the protein was predicted by DeepLoc-1.0. The structure and function of the protein and its co-factor were predicted by I-Tasser.^{87–89} The predicted model was further validated⁹⁰ by RAMPAGE,⁹¹ ERRAT,⁹² ProSA,^{93,94} and ProQ.⁹⁵ I-Tasser further predicted the DNA binding nature of the property along with its binding site by comparing the PDB model with that of another Alba protein from *Sulfolobus shibatae*, Ssh10b.

Parasite culture, synchronization and separation of parasite from infected erythrocytes

Pf3D7 strain was cultured following previous protocol.^{96,97} In brief, *P. falciparum* 3D7 is cultured in complete RPMI-1640 (CRPMI) medium, supplemented with 25 mM HEPES, 1.76 g/L sodium bicarbonate, 2 g/L glucose, 50 mg/mL gentamycin, 370 mM hypoxanthine and 5% (w/v) AlbuMaxII, at a 5% hematocrit in tissue-culture flasks with filtered screw caps in low oxygen atmosphere at 37°C. Culture medium was replaced with fresh medium daily. Erythrocytes from O + ve blood were specifically used for the culture.⁹⁸ Giemsa staining was used to determine the parasitemia in the culture. Parasites were isolated by following the standard methods.⁹⁹ Briefly, erythrocytes with ~10% parasitemia were centrifuged at 800 x g for 5 min at room temperature (RT). The pellet was then washed and resuspended with cold phosphate-buffered saline (PBS-137 mM NaCl, 2.7 mM KCl, 5.3 mM Na₂HPO₄ and 1.8 mM KH₂PO₄, pH- 7.4). The pellet was then lysed by resuspending it in an equal volume of 0.05% saponin in PBS and was kept in ice for 15 min. The erythrocyte suspension was centrifuged at 1300 x g for 5 min to obtain the parasites. The parasite pellet was washed with cold PBS and used immediately or stored in liquid nitrogen for future use. The parasite was synchronized using percoll density gradient and 5% D-sorbitol.^{100,101} In brief, the cultured parasite was centrifuged at 500 x g for 5 min at RT. The supernatant was discarded, and the pellet was resuspended in 2.5 mL (5 times the pellet volume) of incomplete RPMI media (IRPMI; CRPMI without AlbuMaxII) to 7–10% hematocrit. Percoll gradient was prepared by diluting 90% percoll in PBS with IRPMI to 2 mL 65% lower layer and 2 mL 35% upper layer. The resuspended pellet was layered over the percoll gradient and centrifuged in a swing-out bucket at 1500 x g for 15 min at room temperature. The ring stage and the uninfected RBCs were found in the pellet, whereas the trophozoite-enriched infected RBCs were recovered at the interface of different concentrations of percoll. These stages were collected in separate tubes. The collected infected RBCs were washed twice with 10 times the volume of IRPMI medium added dropwise while shaking continuously and centrifuged at 500 x g for 5 min at RT. The supernatant was discarded, and the pellet with the infected RBCs was either used for RNA isolation and protein extraction or further culture with sorbitol. For sorbitol synchronization, the pellet with the infected RBCs was resuspended in 2.5 mL of 5% D-sorbitol for 5 min and centrifuged at 500 x g for 5 min at RT. The pellet was then resuspended in an equal volume of CRPMI media with fresh RBCs, and the culture was maintained as mentioned above.

Extraction of RNA from parasite, cDNA preparation and PCR amplification

RNA extraction was made from nearly 1 X 10⁶ parasites/preparation using TRIzol Reagent (Invitrogen, Thermo Scientific TM) using manufacturer's protocol¹⁰² and estimated in MaestroNano Micro Volume Spectrophotometer (Life Teb Gen co, Tehran-Iran). RevertAid First StrandcDNA synthesis kit (Thermo Fisher Scientific Inc.) and oligo-dT₁₈ primer were used to synthesize cDNA following the manual instructions. Freshly prepared cDNA was subjected to a polymerase chain reaction (PCR) based amplification of PfAlba6 (Forward primer 5'-GGATC CAATATAATACCAAATGACG-3' was flanked with BamHI restriction site (underlined), and the reverse primer 5'-CTCGAGTTATTTTTTCTT TATATATATATGA-3' was flanked with XhoI restriction site (underlined) using DreamTaq Green PCR Master Mix (2X) (Thermo Scientific TM).

Real-time PCR

Real-time PCR was performed to check the mRNA expression level of the protein in all the erythrocytic stages and untreated and treated parasites. RNA was isolated from the different intra-erythrocytic stages for stage-specific expression mRNA expression. For the mRNA expression level of *PfAlba6* in untreated and treated parasites, the parasite culture was treated with artemisinin (IC50 4 nM for 48 h). RNA was isolated from vehicle (DMSO) treated set and artemisinin-treated parasites (time-dependent: 12 h, 18 h, 24 h and 48 h). For mRNA expression level of *PfAlba6* during heat stress, parasite cultures were split into two subcultures, one of which was used as a control and kept at 37°C while the second one was incubated at 39°C for 6 h followed by recovery at 37°C for 10 h. RNA was isolated from control, treated and recovered sets. cDNA, prepared from an equivalent amount of the isolated RNA, was used as a template to amplify *PfAlba6*, *PfActinII* and *PfHsp70-x*. *PfActinII* was used as a housekeeping gene, and *PfHsp70-x* was used as a positive control for the heat stress. Primer sequences used for *PfAlba6* were 5'-GGATCCAATATAATACCAAATGAC G-3' (forward) and 5'-CTCGAGTATTTTTCTTTATATATATATGA-3' (reverse). Similarly, primer sequences used for *PfActinII* are 5'-TGGAAAAAATATGGCATCACA-3' (forward) and 5'-GGTACGACCAGAAGAATATAAG-3' (reverse) and that of *PfHsp70-x* are 5'-GGTAAAGATGTTTCCAAAAATTCA-3' (forward) and 5'-GGTATTAAGTATTACGGAATTGATC-3' (reverse). The qPCRs were performed using SYBR green mastermix (Roche) in RocheLightCycler 96 qPCR system where the following cycling conditions were maintained: initial denaturation at 95°C for 10 min followed by 45 cycles of denaturation at 95°C for 10 s, annealing at 45°C for 30 s and extension at 72°C for 10 s with final cooling step was 40°C for 30 s.

Cloning, overexpression and purification of PfAlba6

The amplified gene was cloned in the pET-28a (+) vector (Novagen). The clones were confirmed by Sanger sequencing using T7 promoter primer per the manufacturer's protocol. The plasmid was transformed for protein expression in Rosetta (DE3) pLysS E. coli (Millipore Sigma). The supernatant was subjected to Fast Pressure Liquid Chromatography (FPLC) (ÅKTA pure protein purification system, GE Healthcare Life Sciences) using cation exchange HiTrap SP FF column (GE Healthcare Life Sciences). Cation exchange purification was started with a buffer of pH 7.5, which is lower than the pI of the protein (9.33). The collected fractions were checked on 15% SDS-PAGE to determine the purity of the isolated protein fraction. Since the protein has a His-tag, the fractions containing protein of interest were further pooled and subjected to Ni-NTA column affinity chromatography to obtain a purified single band. The purified protein was finally eluted with elution buffer (50 mM Tris, 200 mM NaCl and 300 mM imidazole, pH 7.5) and collected in separate 2 mL tubes and run on 15% SDS-PAGE to check the purity and the fractions having the protein. The purified fractions were pooled, concentrated and subjected to size exclusion chromatography using HiLoad Superdex 16/600 75 µg preparative size exclusion chromatography column to remove imidazole. The eluted fractions were collected and again subjected to 15% SDS-PAGE to check the purity of the protein.

Matrix-Assisted Laser Desorption/Ionization- time of Flight (MALDI-TOF) mass spectroscopy

MALDI-TOF mass spectrometry was used to determine the whole protein mass and identify the protein. The protein was passed through the desalting column (Thermo Scientific Zeba Spin Desalting Columns, 7K MW Cut Off, 0.5 mL), and its whole mass and purity were determined using MALDI-ToF MS (MALDI III machine (Shimadzu, Duisburg, Germany) using α -cyano hydroxyl cinnamic acid (CHCA) as a matrix. For further characterization and identification of the protein and to rule out the expression of any other protein or presence of any contaminants of the same molecular mass, MALDI-ToF MS/MS was performed using In-Gel Tryptic Digestion Kit (Thermo Scientific) following the manufacturer's protocol. The digested fraction was concentrated and purified using ZipTip with 0.6 µL C18 resin (Millipore, Sigma-Aldrich) following the manufacturer's protocol. The purified sample was then analyzed upon CHCA as a matrix for MALDI-ToF MS/MS.

Circular dichroism spectroscopy

To determine the secondary structure of PfAlba6, 0.25 mg/mL protein was diluted in phosphate buffer (10 mM Potassium Phosphate, 50 mM KCl), and scanning was performed from 250 nm to 200 nm in mdeg in Jasco J810 spectropolarimeter using 0.1 cm cuvette. Background noise was reduced by scanning the only buffer in the same range under the same condition. The CD spectrum was analyzed in BeStSel.¹⁰³

Antibody generation

Antibody against PfAlba6 was generated in rabbits following the standard protocol.¹⁰⁴ An 8 to 10-month-old rabbit was immunized with purified PfAlba6 protein five times at two-week intervals after each immunization. The first immunization was done by homogeneous emulsion of protein and Freund's complete adjuvant (Sigma Aldrich) in a 1:1 v/v ration such that the final protein concentration becomes 1 mg/ml and immunized via subcutaneous route at four places per animal (0.25 mL each). The subsequent immunization was done by homogeneous emulsion of the protein with Freund's incomplete adjuvant in the same way as above. After 72 days of the first immunization, blood was drawn through the central ear artery of the rabbit and the straw-yellow colored serum was collected. The total IgG of the serum was purified using Protein A Mag Sepharose Xtra (GE Healthcare Life Sciences) affinity columns following the manufacturer's protocol. The antibody thus generated was tested by immunoblotting (Figure S1A (inset)).^{104–106} Antibody was generated in rabbits following the norms laid down by the institutional animal ethical committee of CSIR-IICB, registered with the Committee for the Purpose of Control and Supervision of Experiments on Animals (CPCSEA), India (Permit 147/1999/CPCSEA).

Immunofluorescence assay

An immunofluorescence study was employed to characterize the localization of the protein. Synchronized parasites were cultured following the protocol discussed above. Synchronized culture of *P. falciparum* was taken, washed in PBS thrice, and then fixed in freshly prepared 4% paraformaldehyde with 0.0075% glutaraldehyde in PBS for 40 min at RT in vertical rotor. The culture was then washed with PBS thrice and permeabilized with 0.1% Triton X-100 in PBS for 10 min at RT. Permeabilized infected RBC was then treated with freshly prepared 0.1 mg/mL sodium borohydride in PBS and incubated for 10 min at RT. It was then washed with PBS thrice and blocked with 3% BSA in PBS for 1 h at RT in a vertical rotor. Parasites were then incubated with rabbit anti-PfAlba6 antibody, diluted 1:200 times in 3% BSA in PBS overnight (16 h) at 4°C. After that, the cells were washed three times with PBS and incubated with Alexa Fluor 647 tagged goat anti-rabbit IgG (Molecular Probes, Invitrogen) 1:1000 times diluted in blocking solution (3% BSA in PBS) for 30 min in dark at RT. The tubes were then centrifuged; the pellet was resuspended in the 150 μ L spare supernatant, spread on freshly poly-L-lysine coated coverslips, and incubated in the dark for 30 min. The coverslips were washed with PBS thoroughly, mounted in ProLong Diamond Antifade Mountant with DAPI (Invitrogen, Thermo Scientific) and sealed with nail polish. The slides were then viewed under the 63X oil immersion objective of the Leica TCS-SP8 confocal microscope with a thermo-regulated stage in a 5% CO₂ environment. Images were optically zoomed by around 7X during the capture, and post-capture processing was performed using the LAS X suite (Leica software).

Agarose gel shift assay

DNA binding activity of PfAlba6 was determined by using agarose gel retardation assay following previously published protocol.^{31,49} In brief, supercoiled pBR322 DNA (500 ng) was incubated with the increasing concentrations of purified PfAlba6 protein in binding buffer (20 mM MES, pH 6.5, 100 mM potassium glutamate, 1 mM MgCl₂ and 0.1 mg/mL bovine serum albumin). After incubation for 15 min at 20°C, the DNA protein mix was electrophoresed in 1% agarose gel in 1 X TBE at 70 V. After the electrophoresis, the gel was stained with ethidium bromide (10 mg/mL) and visualized in the GelDoc XR system (Biorad).

Bio-layer interferometry (BLI)

Bio-layer interferometry is a label-free bio-sensor method that provides information on binding, kinetics, concentration, and interaction affinity.¹⁰⁷ It provides real-time monitoring of interactions between an immobilized ligand and an analyte without flow cells. The kinetics of binding affinity dsDNA and PfAlba6 was determined using the Octet RED96 instrument (Pall FortéBio, USA) as previously described.¹⁰⁸ Before analysis, the Streptavidin (SA) kinetic grade biosensor (Pall FortéBio) was hydrated in the kinetics buffer (25 mM Tris, 150 mM NaCl, pH-7.5). The assay was performed at 298 K with continuous shaking at 1000 rpm in 200 μ L reaction volume.¹⁰⁹ Here, 44 ng/ μ L 5'-biotinylated 28 bp DNA (obtained by annealing equimolar 5'-Biotin-TGGCGAAAGGGGGTTGTGCTGCAAGGCG-3' against its complementary strand) was used as bait to immobilize at the tip of SA sensor and varying concentrations of purified PfAlba6 and its mutated variant PfAlba6 Y28A (1 μ M, 0.5 μ M, 0.25 μ M, 0.125 μ M, 0.0625 μ M) were used as analytes separately. The assay steps were equilibration (300 s), binding of 44 μ g/mL biotinylated-DNA (300 s), baseline stabilization (120 s), ligand-analyte association (300 s) and ligand-analyte dissociation (600 s) and regeneration of the sensors with 0.3% SDS (1200 s). The kinetic parameters were determined from the acquired data by Octet Software using global fitting, specifying a 2:1 kinetic model.

Atomic force microscopy (AFM)

Oligomerization of the protein interacting with the DNA was determined using Atomic Force Microscopy (Pico plus 5500 ILM AFM (Agilent Technologies USA) operating in AAC mode). Microfabricated silicon cantilevers with resonance frequencies of 150–300 kHz and spring constants of 21–98 N/m were used to take images at scan speeds of 2 lines/second. The images were processed using Pico View 1.1 version software. Here, the control DNA (pBR322) was viewed without the protein. Purified protein was also visualized in the absence of the DNA. The DNA-protein complex was then used to visualize the increased height of the protein interacting with DNA. Nuclease-free water, filtered protein and MgCl₂ were used for the experiment.

Preparation of APTES-modified MICA

Mica was freshly cleaved and modified with 3-aminopropyltriethoxysilane (APTES) using vaporization method, where 40 μ L was kept at the base of a 50 mL falcon and freshly cleaved surface of MICA was dropped into it, such that it should not touch the solution and thus is being exposed to its vapor and incubated in the dark for 1 h. The MICA was removed after that and was used for DNA immobilization.

Preparation of pBR322 sample

pBR322 was diluted in the nuclease-free water to a final concentration of 10 p.m. in 10 μ L solution. MgCl₂ was added at a final concentration of 12.5 nM mixed, put a drop at the center of the freshly APTES treated MICA, and kept there for 3 min. The MICA was then washed slowly with 3mL water added dropwise with the help of a 1mL syringe. The sample was then dried and viewed.

Preparation of the protein sample

For visualization of the protein sample, no APTES treatment of the MICA was required. 5 μ L of the protein sample at a final concentration of 100 nM diluted in the nuclease-free water was added, air dried and viewed directly.

Preparation of Protein-DNA interacting samples

pBR322 and PfAlba6 in the above concentrations were mixed and incubated for 10 min. 12.5 nM MgCl₂ was added, and the solution was then added to the freshly APTES-treated MICA for 3 min. The MICA was then slowly washed with 3 mL water added dropwise with the help of a 1 mL syringe. The sample was dried and viewed.

DNase activity of PfAlba6

Deoxyribonuclease activity of PfAlba6 was determined by incubating 0.5 µg pBR322 with increasing concentrations of PfAlba6 in 1 X DNase buffer (50 mM Tris-HCl, 10 mM MgCl₂, 100 mM NaCl, pH = 8.0) in a 10 µL reaction at 37°C for 1 h.¹¹⁰⁻¹¹² The reaction is stopped by adding 2 µL 6X loading buffer (NEB B7024S) and electrophoresed in 1% agarose gel in 1X TBE at 70 V. After the electrophoresis, the gel was stained with ethidium bromide (10 mg/mL) and visualized in the GelDoc XR system (Biorad).

Metal ion - Dependency on the DNase activity of PfAlba6

Dependency of the metal ion on the DNase activity of PfAlba6 was determined by carrying out the DNase activity as mentioned by incubating 0.5 µg of pBR322 with 2.5 µg of PfAlba6 in 1X buffer (50 mM Tris-HCl, 100 mM NaCl, pH = 8.0) and increasing concentrations of metal ions (Mg²⁺, Ca²⁺, Zn²⁺, Cu²⁺, Ni²⁺, Mn²⁺) in a 10 µL reaction at 37°C for 1 h. Further dependency on metal was carried out by performing the above reaction in 1X DNase buffer (50 mM Tris-HCl, 100 mM NaCl, 10 mM MgCl₂, 10 mM CaCl₂, pH = 8.0) with increasing concentrations of EDTA and EGTA. The reaction was stopped by adding 2 µL 6X loading buffer (NEB B7024S) and electrophoresed in 1% agarose gel in 1X TBE at 70 V. After the electrophoresis, the gel was stained with ethidium bromide (10 mg/mL) and visualized in the GelDoc XR system (Biorad).

pH - Dependency on DNase activity of PfAlba6

pH dependency on the DNase activity of PfAlba6 was determined by incubating 0.5 µg pBR322 with 2.5 µg PfAlba6 in different pH buffers (pH = 3: 100 mM Sodium Citrate buffer containing 10 mM Mg²⁺, pH = 5: 0.1N Sodium Acetate buffer containing 10 mM Mg²⁺, pH = 7.5: 50 mM Tris, 100 mM NaCl buffer containing 10 mM Mg²⁺, pH = 9: 100 mM Sodium Carbonate/Bicarbonate buffer containing 10 mM Mg²⁺, pH = 10: 100 mM Sodium Carbonate/Bicarbonate buffer containing 10 mM Mg²⁺) in 10 µL reaction at 37°C for 1 h. The reaction is stopped by adding 2 µL 6x loading buffer (NEB B7024S) and electrophoresed in 1% agarose gel in 1X TBE at 70 V. After the electrophoresis the gel was stained with ethidium bromide (10 mg/mL) and visualized in the GelDoc XR system (Biorad).

Temperature-dependency on DNase activity of PfAlba6

Temperature dependency on the DNase activity of PfAlba6 was determined by incubating 0.5 µg pBR322 with 2.5 µg PfAlba6 in 1 X DNase buffer (50 mM Tris-HCl, 10 mM MgCl₂, 100 mM NaCl, pH = 8.0) at different temperatures (37°C, 50°C, 60°C, 70°C) in 10 µL reaction for 1 h. The reaction is stopped by adding 2 µL 6X loading buffer (NEB B7024S) and electrophoresed in 1% agarose gel in 1X TBE at 70 V. After the electrophoresis the gel was stained with ethidium bromide (10 mg/mL) and visualized in the GelDoc XR system (Biorad).

Mutation of PfAlba6

Determining the critical residues involved in the DNase activity will shed some light on its activity mechanism. For this, we performed mutations based on the predictions by I-Tasser. These are the deletion of 19–21 residues (IKS) and site-directed Y mutagenesis at the 28 position to A (Y28A). For this, two pairs of primers were used, as shown in Table S4. Mutations were performed using Agilent Technologies QUIKCHANGE II XL10 REACTIONS (Agilent Technologies 200521) following the manufacturer's protocol (initial denaturation temperature of 95°C for 1 min, 18 cycles of denaturation at 95°C for 50 s annealing at 60°C for 50 s, extension at 68°C for 6 min followed by a final extension at 68°C for 7 min). pET28a - PfAlba6 construct was used as a template. Mutations were further verified by DNA SANGER sequencing.

Successful clones were used to overexpress and purify the mutated proteins (Figure S2A). As previously mentioned, the mutated proteins were then subjected to DNase activity and checked by electrophoresis in 1% agarose gel.

Autoradiography and fluorography

The DNase activity using pBR322 is complicated as it has different types of DNAs in it-closed circular, linear or nicked species. To add to this, pBR322 might also have abasic sites in it. So, to be more specific about the function of PfAlba6, we used small linear 28bp DNA with no abasic sites. For generation of radiolabeled 28bp control DNA with no abasic site, (C28): 5'-TGGCGAAAGGGGGTTGTGCTGCAAGGCG-3' was radiolabeled on the 5' end with [γ - P³²] ATP using T4 polynucleotide kinase (NEB M0201S)^{113,114} following the manufacturer's protocol. A part of this was kept unannealed to be used as ssDNA. The rest of the strand was then annealed to its complementary strand by boiling in water at 100°C for 2 min and then cooling slowly to 4°C to obtain C28. The unincorporated radiolabeled ATP was removed by Zeba Spin Desalting Columns, 7K MWCO, 0.5 mL (ThermoFisher Scientific, Cat: 89882), which was equilibrated with the DNase buffer following the manufacturer's protocol. The specific radioactivity, as determined by a liquid scintillation counter, was approximately, 500000 c.m.p.m/0.1 pmol. To obtain 5' Fluorophore tagged C28 (FAM-C28), FAM (Fluorescein amidite) labeled 5'-TGGCGAAAGGGGGTTGTGCTGCAAGGCG-3' was annealed against its complementary strand as discussed above. To further check if it has any AP endonuclease activity, radiolabeled 28bp DNA containing THF (tetrahydrofuran) at the 14th position (THF28) which mimics the abasic site was prepared by annealing 5'-FAM labeled 5'-TGGCGAAAGGGGGTHTGTGCTGCAAGGCG-3' against 3'-ACCGCTTCCCCGACACGA CGTCCGC-5'. To further determine the

directionality of the DNase activity, 3' FAM (Fluorescein) labeled 5'-TGGCGAAAGGGGGTHFTGTGCTGCAAGGCG-3' was annealed against 3'-ACCGCTTCCCCCGACACGA CGTCCGC-5' to obtain a 3' labeled THF28 (3'-THF28).

To characterize the DNase activity of the protein, 0.1 pmol of FAM-labelled and radiolabeled oligonucleotides C28, THF28, 3'-C28 and ssDNA were treated with 2.5 μ g of PfAlba6 or its mutated variants in 20 μ L reaction volume containing 1X Dnase Buffer (50 mM Tris-HCl, 100 mM NaCl, 10 mM MgCl₂, pH = 8.0) and compared with the DNase activity of PfAlba3 in its DNase buffer (10 mM Tris-HCl, 2.5 mM MgCl₂, 0.5 mM CaCl₂, pH = 7.6), Endo III, Endo IV and DNase I in their respective buffer system provided by the manufacturer. The reaction was terminated by the addition of 20 μ L of 2X formamide loading buffer (95% deionized formamide, 0.05% bromophenol blue, 0.05% xylene cyanol FF, 5 mM EDTA) after incubation for 1 h at 37°C. The samples were then heated at 75°C for 2 min, and roughly 10000 c.p.m was subjected to denaturing (8.3 M Urea) polyacrylamide gel electrophoresis in TBE buffer for 2 h at 55 W constant power. For radioactivity, products were analyzed by autoradiography of semi-dry gels in TyphoonFLA 7000 (GE Healthcare). Fluorophore-labelled gels were analyzed directly in TyphoonFLA 7000 (GE Healthcare).

For determining the enzyme kinetics of PfAlba6, triplicate sets of different C28 concentrations (0.15, 0.3, 0.6, 1.2, 1.8, 2.4, 3.0, 3.6 μ M) incubated with 2 μ g of PfAlba6 in assay buffer (10 mM Tris-HCl, 10 mM MgCl₂, pH 8.0) in a total reaction volume of 10 μ L and subjected to incubation at 37°C for 1 h. The reaction was terminated by the addition of 20 μ L of 2X formamide loading buffer (95% Deionized formamide, 0.05% bromophenol blue, 0.05% xylene cyanol FF, 5 mM EDTA) after incubation for 1 h at 37°C. The samples were then heated at 75°C for 2 min and were subjected to denaturing (8.3 M urea) polyacrylamide gel Electrophoresis in TBE buffer for 2 h at 55 W constant power. The gel was then stained with Invitrogen SYBR Safe DNA Gel Stain per the manufacturer's protocol and visualized in the GelDocXR system (Biorad). The control sets contain the respective amounts of C28 in the assay buffer without PfAlba6. The difference in the fluorescence (measured in A.U.) of DNA-SYBR Safe DNA Gel Stain adduct in the absence and presence of PfAlba6 was calculated through densitometry analysis using ImageJ software. It was used to determine the amount of product formed from a known concentration of DNA. This has been used to determine V_{max} , K_M and k_{cat} of PfAlba6.

Real-time assay of DNase activity

The real-time DNase activity of the protein was determined in a fluorometer using PicoGreen dye (Quant-iT PicoGreen dsDNA Reagent P11495). PicoGreen, having emission/excitation at 485/525, binds to the dsDNA and forms a highly luminescent complex compared to when free. Time-dependent DNase activity of the protein was carried out by recording the wavelength scan in Hitach F-7000 Fluorescence Spectrophotometer from 500 to 600 nm at time 0 min, 2 min, 5 min, 10 min, 15 min, 20 min, 30 min, 45 min and 60 min. As the protein cleaves the DNA, PicoGreen becomes free, and its intensity decreases.¹¹⁵ Thus, we can monitor the DNase activity in real-time. PicoGreen assay was performed to compare the activity of PfAlba6 and PfAlba6 Y28A.

QUANTIFICATION AND STATISTICAL ANALYSIS

All statistical analyses were performed using GraphPad Prism 5.0 (GraphPad Software). The respective figure legends gave detailed information about statistical analysis, including statistical tests (two tailed paired t-tests) performed to determine p values and mean \pm SEM, biological and technical replicates, and statistical methods for individual experiments.